Journal of Molecular Liquids 223 (2016) 572–588

Contents lists available at ScienceDirect

Journal of Molecular Liquids

journal homepage: www.elsevier.com/locate/molliq

Nanofluid flow and heat transfer around a circular cylinder: A study on effects of uncertainties in effective properties

R. Deepak Selvakumar, S. Dhinakaran *

The Center for Fluid Dynamics, Discipline of Mechanical Engineering, Indian Institute of Technology Indore, Khandwa Road, Simrol, Indore 453 552, Madhya Pradesh, India

ARTICLE INFO

Article history:
Received 18 December 2015
Accepted 13 August 2016
Available online 22 August 2016

Keywords:
Nanofluids
Circular cylinder
Heat transfer
Effective properties
Uncertainties
Finite-volume method

ABSTRACT

Nanofluids are considered to be the coolants of future; in the interest of their enhanced thermal conductivity. But, the dilemma in prediction of their effective properties is a major problem in assessing their real heat transfer potential. A numerical analysis of flow and heat transfer from a hot circular cylinder exposed to an uniform stream of nanofluid has been performed to showcase the effects of uncertainties in effective properties of nanofluids. Water based nanofluids with ultra-fine Titania (TiO_2) nanoparticles with the particle volume fraction varying from 0% to 2% have been considered. A steady, laminar, 2-D flow with forced convective heat transfer has been taken into account in the Reynolds number range of $1 \leq Re \leq 40$. Finite-volume method based on SIMPLE algorithm is used to solve the governing equations. Three cases of analysis have been carried out in which the thermal conductivity and viscosity of nanofluids are determined using two sets of theoretical models and one set of experimental thermal conductivity and viscosity data from literature, respectively. Flow and heat transfer characteristics of nanofluids are found to be dependent on particle volume fraction and Reynolds number. Enhanced drag, altered wake lengths, modified flow separation and higher heat transfer rates are seen in nanofluids. But, a comparative scrutiny of the three cases; apparently shows that the flow and heat transfer characteristics differ both quantitatively and qualitatively between each case. This work promulgates the importance of a precise effective thermal conductivity and viscosity models for nanofluids to promote the real time application of nanofluids in developing high efficiency heat transfer systems.

1. Introduction

With the advent of high power and miniature devices, efficient heat removal has become indispensable to achieve the desired performance and reliable functioning of numerous products ranging from high functionality palm tops to huge automobile engines. Thus, development of energy efficient heat transfer systems has become the top priority in many high-tech industries. Heat transfer techniques which are being used widely at present; such as increasing the surface area by fins, micro-channel cooling and dual phase cooling techniques have already reached their limits due to the poor intrinsic thermal conductivities of conventional heat transfer liquids. Due to this pressing need for new and innovative cooling liquids, the novel concept of nanofluids, i.e., cooling liquids suspended with fine nanoparticles, was developed [1]. Nanofluids, by virtue of their enhanced and adjustable thermo-physical properties, find real-time applications in several heat transfer and energy systems [2–5]. Hence, analysis of flow and heat transfer characteristics of nanofluids has become a trending topic among researchers [6–17].

Many industrial applications like power electronics cooling, heat exchangers, chimney stacks, cooling towers, power generators and nuclear reactor fuel element cooling, etc., mimic the flow around circular cylinders [18]. For instance, a setting of nuclear fuel element cooling involving flow around circular cylinders is shown in Fig. 1. Owing to the enhanced effective properties of nanofluids and numerous heat transfer applications, numerical analysis of flow and heat transfer around cylinders using nanofluids has become an active area of research. Nanofluids due to their different effective thermo-physical properties exhibit modified flow and heat transfer characteristics. Valipour and Ghadi [19] numerically analyzed the forced convective heat transfer around a solid circular cylinder using nanofluids. The effective thermal conductivity and viscosity of nanofluids were determined using Hamilton-Crosser model [20] and Brinkman model [21], respectively. Nanofluids exhibited stronger vorticity and enhanced heat transfer rates. A similar study on forced convective heat transfer past a square cylinder by Valipour et al. [22] also confirmed their observations on circular cylinder. A numerical study on forced convective nanofluid flow around a circular cylinder by Vegad et al. [23] in which the effective properties were calculated using Maxwell-Garnett model [24] and Brinkman model [21] also showed synonymous results. Abu-Nada et al. [25] in their numerical study on mixed convective heat transfer around a circular cylinder showcased that the heat transfer enhancement is dependent on

* Corresponding author.
E-mail address: ssdhinakar@gmail.com (S. Dhinakaran).

http://dx.doi.org/10.1016/j.molliq.2016.08.047
0167-7322/

Nomenclature

Notations

C_D	Drag coefficient, $\frac{F_D}{0.5\rho_f U_\infty^2 2a}$
c_p	Specific heat capacity, $[J Kg^{-1}K^{-1}]$
θ_s	Flow separation angle
p	Dimensional pressure, $[Nm^{-2}]$
r	Dimensional radial coordinate
R_∞	Extent of external boundary
u, v	Dimensional components of velocity, $[ms^{-1}]$
m, n	Number of grids in r and θ direction
Re	Reynolds number, $\frac{\rho_f U_\infty a}{\mu_f}$
Nu_s	Local Nusselt number, $-\frac{k_{eff}}{k_f}\frac{\partial\Theta}{\partial n_s}$
C_P	Pressure coefficient, $\frac{P-P_\infty}{\frac{1}{2}\rho_f U_\infty^2}$
a	Radius of the cylinder
L_r	Wake length
P	Non-dimensional pressure, $\frac{p}{\rho_f U_\infty^2}$
R	Non-dimensional radial coordinate
t	Dimensional time, [s]
U, V	Non-dimensional components of velocity
Pr	Prandtl number, $\frac{\nu_f}{\alpha_f}$
Re_{cr}	Critical Reynolds number
Nu_M	Mean Nusselt number, $\frac{1}{\pi}\int_0^\pi Nu \sin\theta \, d\theta$

Greek symbols

ρ	Density, $[kgm^{-3}]$
μ	Dynamic viscosity, $[kgm^{-1}s^{-1}]$
ω_s	Surface vorticity
Φ	Dependent variable, (U, V, Θ)
Θ^*	Dimensional temperature, [K]
θ^*	Dimensional coordinate
α	Thermal diffusivity, $[m^2s^{-1}]$
ν	Kinematic viscosity, $[m^2s^{-1}]$
ϕ	Nanoparticle volume fraction, [in %]
τ	Non-dimensional time, $\frac{tU_\infty}{a}$
Θ	Non-dimensional temperature, $\frac{(\Theta^*-\Theta_\infty^*)}{\Theta_S^*-\Theta_\infty^*}$
θ	Non-dimensional coordinate

Subscripts

∞	Far field value
S	Surface value
m	Mean or average value
DV	Drag due to viscous forces
f, bf	Fluid or Base fluid
p	Nanoparticle
nf, eff	Effective property of nanofluid
DP	Drag due to pressure forces

thermal conductivity of nanoparticles and particle volume fraction. Bing and Mohammed [26] performed a numerical study on upward laminar mixed convective flow around a circular cylinder and showed that nanofluids with smaller nanoparticles produced higher heat transfer rates. Farooji et al. [27] numerically simulated a laminar nanofluid flow around a circular cylinder and exhibited that there is an optimum particle volume fraction for a given nanoparticle diameter at which the maximum heat transfer will be observed. A numerical analysis of transient natural convective boundary layer flow past a vertical cylinder using nanofluids by Chamkha et al. [28] showcased the dependence of heat transfer enhancement on nanoparticle shape. It was noted that spherical particles are capable of producing higher heat transfer rates. Notable aspect of this work is that, Brownian motion and thermophoresis were considered while determining the effective thermal conductivity of nanofluids. Sarkar et al. [29] made a detailed study on wake dynamics and heat transfer using nanofluids in forced and mixed convective flow past a circular cylinder at high Prandtl numbers. A stabilizing effect in flow and enhanced heat transfer were noted at higher Richardson numbers. Similar results were obtained in a numerical study of mixed convective flow around a circular cylinder using nanofluids [30]. A buoyancy driven mixed convective flow around square cylinder using nanofluids by Sarkar et al. [31] showed that heat transfer is a function of particle volume fraction. Addition of nanoparticles to the basefluid resulted in more number of low frequency higher energy modes in a mixed convection flow around a square cylinder [32]. During a mixed convective vertical flow and heat transfer around a square cylinder using nanofluids, addition of nanoparticles to the basefluid caused a decrease in total entropy generation [33].

In general, there are two approaches for numerically modeling the nanofluid flow and heat transfer. The primary approach is single-phase modeling which considers nanofluids to be a homogeneous fluid with effective properties. It is also hypothesized that the particles and basefluid are in thermal equilibrium and move with same velocity. The second method for modeling nanofluids is the two-phase approach, in which the basefluid and nanoparticles are considered to be heterogeneous and the velocity slip between them is taken into account. Even though articles on two-phase modeling of nanofluids are coming up [34–49], majority of the works available in literature follow single-phase approach due to its simplicity and lesser computational expense [50–52]. Single-phase approach utilizes theoretical models to predict the effective properties of nanofluids. But, review of related literature reveals that there is an inconsistency in prediction of effective properties of nanofluids. No single model is capable of comprehensively explaining all available experimental data [53]. It is also essential to note that, almost all available works on nanofluid flow around bluff bodies follow single-phase approach, in which available formulas based on

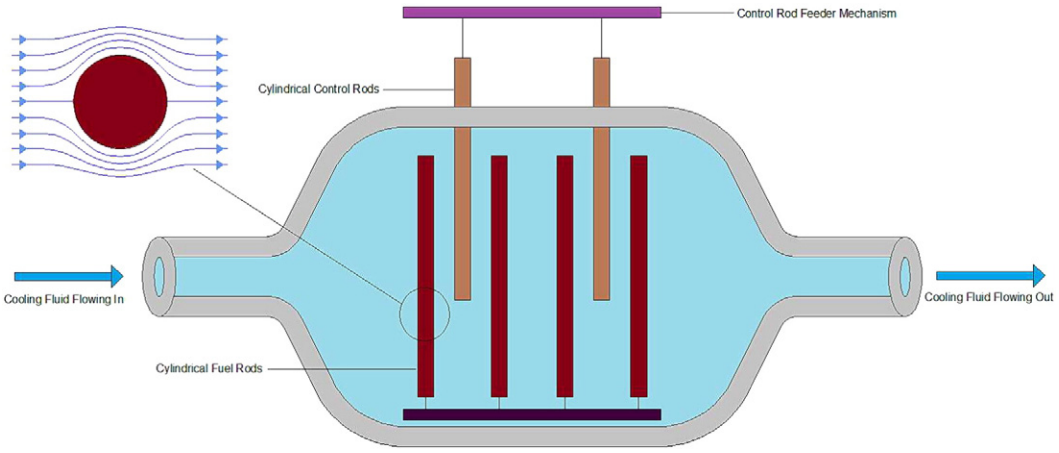

Fig. 1. A simple sketch of a nuclear reactor which involves the flow of coolant around control rods and fuel rods which imitate the scenario of flow around circular cylinders.

classical theory of heterogeneous suspensions have been employed to predict the thermo-physical properties of nanofluids. Classical theory based models were proposed for suspensions of micro and millimeter sized particles and these approximations cause considerable errors in the prediction of nanofluid effective properties and lead to discrepancies while assessing the flow and heat transfer characteristics of nanofluids. Even though few works have considered some recent models, there is an uncertainty prevailing in the prediction of effective properties of nanofluids. No attempt has been made to analyze the effects of these uncertainties on flow and heat transfer characteristics around a circular cylinder during a forced convection scenario. Abu-Nada et al. [54] made a similar attempt; but, their work is concerned only about the Nusselt number variation. A more detailed study is necessary to understand the effects of uncertainties in effective properties of nanofluids on different flow and heat transfer characteristics.

1.1. Objectives of this study

In this work, we highlight the effects of uncertainties in effective properties of nanofluids on flow and heat transfer characteristics during an unconfined forced convective flow around a circular cylinder. The flow is considered to be laminar, steady and two-dimensional with the Reynolds number varying from 1 to 40. TiO_2-water nanofluid with particle volume fraction varying from 0% to 2% have been used for analysis. Titania (TiO_2) nanoparticles are chosen because they exhibit better stability even without addition of any external stabilizing agents [55]. The volume fraction is limited to a maximum of 2%, considering the pumping power increase observed at high particle volume fractions. At the considered particle volume fraction, water based nanofluids show no remarkable increase in pumping power [56]. To quantify the effects of uncertainties in effective properties on heat transfer and flow characteristics; three cases are considered, in which the effective thermal conductivity and viscosity of nanofluids are determined from different theoretical models and experimental thermal conductivity and viscosity data from literature [21,57–60]. The particle size is considered to be 21 nm and the temperature is assumed to be 25 °C in Case 2 to match with the experimental data considered in Case 3. A much more detailed elaboration of all three cases is presented in Section 2.4.

Layout of this paper is as follows: The problem and geometrical configuration are clearly explained in Section 2.1. Definition of model formulation by reviewing governing equations for 2-D incompressible flow and heat transfer have been presented in Section 2.2. In Section 2.4, the calculations of thermo-physical properties in each case are presented clearly. Important flow and heat transfer parameters studied in this work are defined in Section 2.5. A detailed description of the numerical procedure, grid generation, grid independence study and code validation are presented in Section 2.6. An elaborate discussion and a comparative analysis on all three cases of simulations are made in Section 3. Finally, concluding remarks on the analysis and the effects of uncertainties in effective properties of nanofluids on flow and heat transfer characteristics have been presented in Section 4.

2. Mathematical formulation

2.1. Problem definition and geometrical configuration

An infinitely long cylinder of circular cross section with radius (a) is considered. The cylinder is considered to be at both classical temperature boundary conditions (Constant Wall Temperature (CWT) and Uniform Heat Flux condition (UHF)) and exposed to nanofluid flowing with an uniform free stream velocity (U_∞), which is at an ambient temperature (Θ^*_∞). The center of the cylinder is considered to be at the origin of the cylindrical co-ordinate system (r, θ) and the uniform stream of nanofluid is directed towards the positive x-direction. The flow is considered to be two-dimensional as the cylinder is infinitely long. The cylinder is considered to exchange heat with the surrounding nanofluid stream. The outer boundary is placed at a sufficient distance ($100a$) far-away from the cylinder surface in order to make the problem computationally feasible. Fig. 2 shows a clear picture of the computational domain used in this work.

2.2. Governing equations

Nanofluids considered in this analysis are very dilute suspensions of nanoparticles of very small size (21 nm). As the particle size is very small, they become homogeneous and behave like basefluid. There is no motion slip between the particles and the liquid phase. Particles and liquid elements are in thermal equilibrium [19]. With all these assumptions, nanofluids are treated as pure fluids with effective properties and the governing equations of pure fluids are applied for nanofluids [61]. Nanofluids in the particle volume fraction range considered in this study exhibit Newtonian behavior [60]. Thus, the continuity, momentum and energy equations for Newtonian fluid are solved in the dimensional form as follows, assuming that the viscous dissipation is negligible.

Continuity equation:

$$\frac{1}{r}\frac{\partial}{\partial r}(rv) + \frac{1}{r}\frac{\partial}{\partial \theta^*}(u) = 0 \tag{1}$$

Momentum equations:

$$\rho_{nf}\left(\frac{\partial u}{\partial t}+\frac{u}{r}\frac{\partial u}{\partial \theta^*}+v\frac{\partial u}{\partial r}+\frac{uv}{r}\right) = -\frac{1}{r}\frac{\partial p}{\partial \theta^*}+\mu_{eff}\left(\frac{1}{r}\frac{\partial}{\partial r}\left(r\frac{\partial u}{\partial r}\right) + \frac{1}{r^2}\frac{\partial^2 u}{\partial \theta^{*2}} + \frac{2}{r^2}\frac{\partial v}{\partial \theta^*} - \frac{u}{r^2}\right) \tag{2}$$

$$\rho_{nf}\left(\frac{\partial v}{\partial t}+\frac{u}{r}\frac{\partial v}{\partial \theta^*}+v\frac{\partial v}{\partial r}-\frac{u^2}{r}\right) = -\frac{\partial p}{\partial r}+\mu_{eff}\left(\frac{1}{r}\frac{\partial}{\partial r}\left(r\frac{\partial v}{\partial r}\right)+\left(\frac{1}{r^2}\frac{\partial^2 v}{\partial \theta^{*2}}\right)-\frac{2}{r^2}\frac{\partial u}{\partial \theta^*}-\frac{v}{r^2}\right) \tag{3}$$

Energy equation:

$$(\rho c_p)_{nf}\left(\frac{\partial \Theta^*}{\partial t} + \frac{u}{r}\frac{\partial \Theta^*}{\partial \theta^*} + v\frac{\partial \Theta^*}{\partial r}\right) = k_{eff}\left[\frac{1}{r}\frac{\partial}{\partial r}\left(r\frac{\partial \Theta^*}{\partial r}\right) + \frac{1}{r}\frac{\partial}{\partial \theta^*}\left(\frac{1}{r}\frac{\partial \Theta^*}{\partial \theta^*}\right)\right] \tag{4}$$

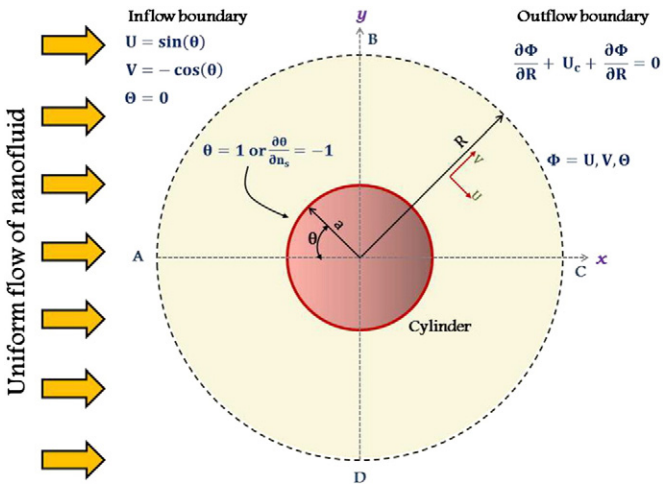

Fig. 2. Schematic representation of uniform flow of nanofluid around a hot circular cylinder with Constant Wall Temperature (CWT) and Uniform Heat Flux (UHF) condition applied on the cylinder surface.

The governing equations of flow and heat transfer can be non-dimensionalized by using the following characteristics scales:

$$U=\frac{u}{U_\infty};V=\frac{v}{U_\infty};\theta=\theta^*;R=\frac{r}{a};\tau=\frac{tU_\infty}{a};$$
$$P=\frac{p}{\rho_f U_\infty^2};\Theta=\frac{(\Theta^*-\Theta_\infty^*)}{(\Theta_s^*-\Theta_\infty^*)}$$

The governing equations for incompressible flow and heat transfer in forced convective regime past a circular cylinder can be expressed in dimensionless form as follows:

Continuity equation:

$$\frac{1}{R}\frac{\partial}{\partial R}(RV)+\frac{1}{R}\frac{\partial}{\partial\theta}(U)=0 \tag{5}$$

Momentum equations:

$$\frac{\partial U}{\partial\tau}+\left(\frac{U}{R}\frac{\partial U}{\partial\theta}+V\frac{\partial U}{\partial R}+\frac{UV}{R}\right)=-\frac{\rho_f}{\rho_{nf}}\frac{1}{R}\frac{\partial p}{\partial\theta}+\frac{2}{\nu_f Re}\frac{\mu_{eff}}{\rho_{nf}}\left(\frac{1}{R}\frac{\partial}{\partial R}\left(R\frac{\partial U}{\partial R}\right)+\left(\frac{1}{R^2}\frac{\partial^2 U}{\partial\theta^2}\right)+\frac{2}{R^2}\frac{\partial V}{\partial\theta}-\frac{U}{R^2}\right) \tag{6}$$

$$\frac{\partial V}{\partial\tau}+\left(\frac{U}{R}\frac{\partial V}{\partial\theta}+V\frac{\partial V}{\partial R}-\frac{U^2}{R}\right)=-\frac{\rho_f}{\rho_{nf}}\frac{\partial P}{\partial R}+\frac{2}{\nu_f Re}\frac{\mu_{eff}}{\rho_{nf}}\left(\frac{1}{R}\frac{\partial}{\partial R}\left(R\frac{\partial V}{\partial R}\right)+\left(\frac{1}{R^2}\frac{\partial^2 V}{\partial\theta^2}\right)-\frac{2}{R^2}\frac{\partial U}{\partial\theta}-\frac{V}{R^2}\right) \tag{7}$$

Energy equation:

$$\frac{\partial\Theta}{\partial\tau}=\left(\frac{U}{R}\frac{\partial\Theta}{\partial\theta}+V\frac{\partial\Theta}{\partial R}\right)=\frac{\alpha_f}{\alpha_{nf}}\frac{2}{Re\,Pr}\left[\frac{1}{R}\frac{\partial}{\partial R}\left(R\frac{\partial\Theta}{\partial R}\right)+\frac{1}{R}\frac{\partial}{\partial\theta}\left(\frac{1}{R}\frac{\partial\Theta}{\partial\theta}\right)\right] \tag{8}$$

Here, $\alpha=\frac{k}{\rho c_p}$ is the thermal diffusivity with subscripts 'nf' and 'f' corresponding to nanofluid and pure fluid. Reynolds number and Prandtl number are given as $Re=2aU_\infty/\nu_f$ and $Pr=\nu_f/\alpha_f$, respectively.

2.3. Boundary conditions

Following are the conditions applied at various boundaries (see Fig. 2) in order to solve the flow problem.

2.3.1. Inflow boundary (AB)

At the inflow boundary an uniform flow in x-direction and uniform fluid temperature are assumed. i.e.,

$$U=U_\infty\sin\theta;V=U_\infty\cos\theta\text{ and }\Theta=0\left(\text{when, }R=R_\infty\text{ and }0\le\theta\le\frac{\pi}{2};\frac{3\pi}{4}\le\theta\le2\pi\right)$$

2.3.2. Outflow boundary (BC)

Convective boundary condition has been used as it decreases the number of time steps and allows smaller length of outer boundary (R_∞) to be used [62,63]

$$\frac{\partial\Phi}{\partial\tau}+U_c\frac{\partial\Phi}{\partial R}=0\left(\text{when, }R=R_\infty\text{ and }\frac{\pi}{2}\le\theta\le\frac{3\pi}{2}\right)$$

where, U_c is the average non-dimensional streamwise velocity (equal to unity) and Φ is the dependent variable U,V or Θ.

2.3.3. On the cylinder surface

No-slip velcoity condition and both CWT and UHF temperature conditions are applied on the cylinder surface i.e.,

$$U=0;V=0\text{ and }\Theta=1\ (CWT)\ \&\ \frac{\partial}{\partial n_s}=-1\ (UHF)\ (\text{when, }R=a\text{ and }0\le\theta\le2\pi)$$

2.4. Thermo-physical properties of nanofluids

The thermo-physical properties of nanoparticle and the basefluid are listed in Table 1. In this study, we adopt a single phase approach in which the nanofluid is assumed to be a homogeneous liquid with effective physical properties.

2.4.1. Effective thermal conductivity and viscosity

We consider three different cases and in each case the effective thermal conductivity and viscosity of nanofluid are calculated differently. Each case is explained in detail as follows:

Case 1 - Initially, for the first case; we consider the effective thermal conductivity of nanofluids given by MG model [57]

$$k_{eff}=k_f\left[\frac{(k_p+2k_f)-2\phi(k_f-k_p)}{(k_p+2k_f)+\phi(k_f-k_p)}\right] \tag{9}$$

The effective viscosity of nanofluids is calculated by Brinkman model [21] as

$$\mu_{eff}=\frac{\mu_f}{(1-\phi)^{2.5}} \tag{10}$$

Case 2 - In the second case, we consider the upper limit of effective thermal conductivity of nanofluids proposed by Murugesan et al. [58].

$$\frac{k_{eff}}{k_f}=\frac{k_p+(n-1)k_f+(n-1)(1+\beta)^3\phi(k_p-k_f)}{k_p+(n-1)k_f-(1+\beta)^3\phi(k_p-k_f)}+C\frac{\phi(T-T_0)}{\mu_f d_p{}^4 k_f} \tag{11}$$

where, $\beta=\frac{\delta}{d_p}$, δ is the thickness of the nanolayer which is assumed as 1 nm and $C=7\times10^{-36}$ (empirical constant) [58]. n is the shape factor which is equal to 3 for spherical particles [58]. T_0 is the reference temperature and is equal to 20 °C and T is the temperature at which the thermal conductivity is measured. In this study T is considered as 25 °C. d_p is the particle diameter which is taken as 21nm.

We consider a correlation proposed by Chen et al. [59] to predict the effective viscosity in Case 2.

$$\mu_{eff}=\mu_f\left(1+10.6\phi+(10.6\phi)^2\right) \tag{12}$$

This correlation is based on an experimental data which takes into account the effect of particle aggregation and Brownian motion.

Case 3 - Finally, we take into account the experimental values of effective thermal conductivity and viscosity of nanofluids [60] which contain ultra-fine Titania(TiO_2) nanoparticles of size 21nm suspended in water as basefluid. The measurements were made at a temperature of 25°C. The data are tabulated in Table 2.

Table 1
Thermo-physical properties of TiO_2 nanoparticle and H_2O (water) basefluid.

S·No	Material	k in W/mK	μ_f in $mPa.S$	ρ in kg/m^3	C_p in J/kgK
1	TiO_2	11.700	–	4230	711.7556
2	Water	0.5800	0.000891	997.047	4181.0

Table 2
Experimental data for effective thermal conductivity and viscosity of TiO_2-water nanofluid from literature [60].

TiO_2 - water, temperature = 25°C, particle diameter = 21 nm [60]			
S·No	ϕ in %	k_{eff} in W/mK	μ_{eff} in kg/mS
1	0	0.5800	0.0008910
2	0.2	0.6104	0.0009185
3	0.6	0.6174	0.0009379
4	1	0.6202	0.0009757
5	1.5	0.6321	0.0009990
3	2	0.6367	0.0010110

2.4.2. Choice of effective thermal conductivity and viscosity models

In the first case, we choose Maxwell-Garnett model [57] for the prediction of effective thermal conductivity of nanofluids. This is a primary model for prediction of effective thermal conductivity of heterogeneous suspensions. This model expresses the effective thermal conductivity as a function of intrinsic thermal conductivities of components and nanoparticle volume fraction. This model is valid only for a dilute suspension of spherical particles. The effective viscosity of nanofluid is predicted by the basic Brinkman model [21]. In this model, the effective viscosity is expressed as a function of basefluid viscosity and nanoparticle volume fraction. Some review and experimental studies available in literature confirm the classical nature of heat transport in nanofluids [64,65]. It means that the thermal conductivity enhancement observed in nanofluids are well explained by Effective Medium Theory (EMT) based models. An experimental study by Xuan and Li [56] indicate that the effective viscosity of nanofluids match well with the Brinkman theory. These observations from the literature indicate that these basic models cannot be neglected completely. Hence, in the first case; we consider these two basic models to predict the effective thermal conductivity and viscosity. Many numerical works available in literature have used these models [22,25,27,29]. More recently, Sarkar et al. [32] have used this approach to study the nanofluid flow around bluff bodies.

In the second case, we consider the upper limit for effective thermal conductivity of nanofluids proposed by Murugesan et al. [58]. This model considers the influence of Brownian motion and interfacial layer formation along with the effective medium theory. This model is capable of explaining the particle shape and size dependence of effective thermal conductivity of nanofluids. Temperature dependence of effective thermal conductivity is also explained by this model. In this case, the effective viscosity of nanofluids is predicted using a correlation proposed by Chen et al. [59] which takes into account the clustering of nanoparticles. A theoretical work by Keblinski et al. [66] indicate that the heat transport in nanofluids are influenced by Brownian motion and interfacial layer formation. Thus, it is meaningful to choose the upper limit of effective thermal conductivity of nanofluids, assuming that the nanofluid considered in this study exhibits Brownian motion and interfacial layer formation.

In the third case, we utilize experimental data for effective thermal conductivity and viscosity of TiO_2-water nanofluids from literature [60], where the particles were of 21nm in diameter and the measurements were made at a temperature of 25 °C.

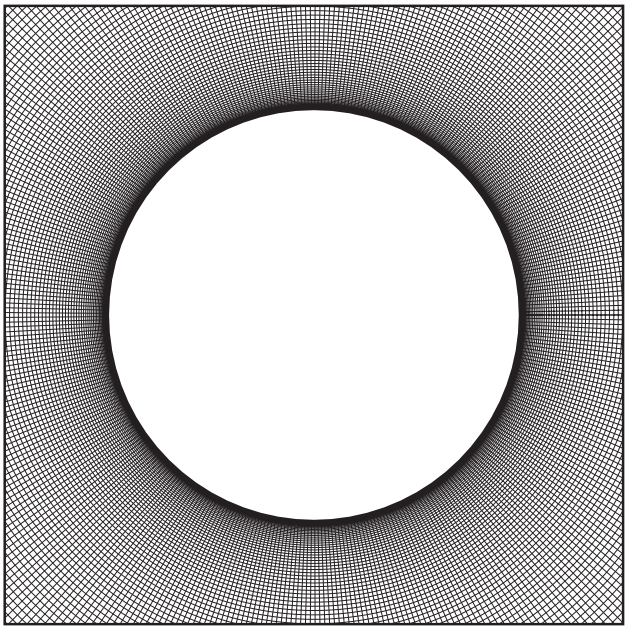

Fig. 3. Close view of mesh distribution around the circular cylinder.

Table 3
Grid independence study.

S·No	$(m\times n)$	(R_∞)	C_D	% Difference	Nu_M	% Difference
1	199 × 545	50	1.5276	0.22	3.2730	0.003
2	401 × 545	50	1.5310	0.08	3.2731	0.003
3	601 × 545	50	1.5323	–	3.2732	–
4	199 × 745[a]	100	1.5060	0.21	3.2609	0
5	401 × 745	100	1.5092	0.07	3.2609	0.003
6	601 × 745	100	1.5103	–	3.2610	–
7	199 × 945	150	1.5059	0.1	3.2609	0.1
8	401 × 945	150	1.5031	0.07	3.2575	0
9	601 × 945	150	1.5042	–	3.2575	–

[a] Grid used in this study.

2.4.3. Effective density

Apart from the effective thermal conductivity and effective viscosity, density of nanofluid also varies from the base fluid. The effective density of the nanofluid is given as follows:

$$\rho_{eff} = \phi\rho_p + (1-\phi)\rho_f \tag{13}$$

2.4.4. Effective heat capacitance

The effective heat capacitance of nanofluid is given by [56]

$$(\rho c_p)_{eff} = \phi(\rho c_p)_p + (1-\phi)(\rho c_p)_f \tag{14}$$

2.5. Definitions of certain parameters

Some of the parameters used in this study are defined as follows:

2.5.1. Drag coefficient (C_D)

The coefficient of drag of the cylinder is calculated as

$$C_D = \frac{F_D}{0.5\rho_f U_\infty^2 2a} = C_{DP} + C_{DV} \tag{15}$$

where, C_{DP} and C_{DV} represent the drag coefficient due to pressure and

Table 4
Comparison of coefficient of drag C_D for flow around a circular cylinder using air as working fluid with literature.

Re	Present study	Dennis & Chang[a] [72]	Lange et al. [75]	Soares et al. [76]	% Diff
5	4.071	4.1160	4.000	3.950	1.090
10	2.827	2.8460	2.800	2.760	0.640
20	2.040	2.0450	2.000	1.990	0.220
30	1.713	—	—	1.670	—
40	1.522	1.5229	1.500	1.490	0.050

[a] Data used to calculate percentage difference.

Table 5
Comparison of mean Nusselt number Nu_M for flow around a circular cylinder using air as working fluid with literature.

	Constant Wall Temperature (CWT)					Uniform Heat Flux (UHF)				
Re	Present	[69]	[a][76]	[75]	% Diff	Present	[a][69]	[77]	[78]	% Diff
5	1.398	–	1.460	1.390	0.620	1.504	–	–	–	–
10	1.856	1.862	1.860	1.810	2.520	2.034	2.040	2.041	2.146	0.27
20	2.455	2.465	2.430	2.410	1.830	2.768	2.778	2.662	2.863	0.35
30	1.713	–	2.850	2.880	0.640	3.311	–	–	–	–
40	3.267	3.282	3.200	3.280	0.030	3.757	3.775	3.472	3.793	0.47

[a] Data used to calculate percentage difference.

viscous force, respectively. F_D is drag force acting on the cylinder surface. Thus, the drag coefficients due to viscous and pressure force can be obtained from the following expressions.

$$C_{DV} = \frac{2\mu_{\text{eff}}}{\mu_f Re}\int_0^{2\pi} \omega_s \sin\theta \, d\theta; \tag{16}$$

$$C_{DP} = \frac{2\mu_{\text{eff}}}{\mu_f Re}\int_0^{2\pi} C_P \cos\theta \, d\theta. \tag{17}$$

2.5.2. Local Nusselt number (Nu_s)

Local Nusselt number at any point on the cylinder surface is determined as

$$Nu_s = -\frac{k_{\text{eff}}}{k_f}\frac{\partial\Theta}{\partial n_s}(\text{CWT}) \text{ and } Nu = -\frac{k_{\text{eff}}}{k_f}\frac{1}{\Theta}(\text{UHF}) \tag{18}$$

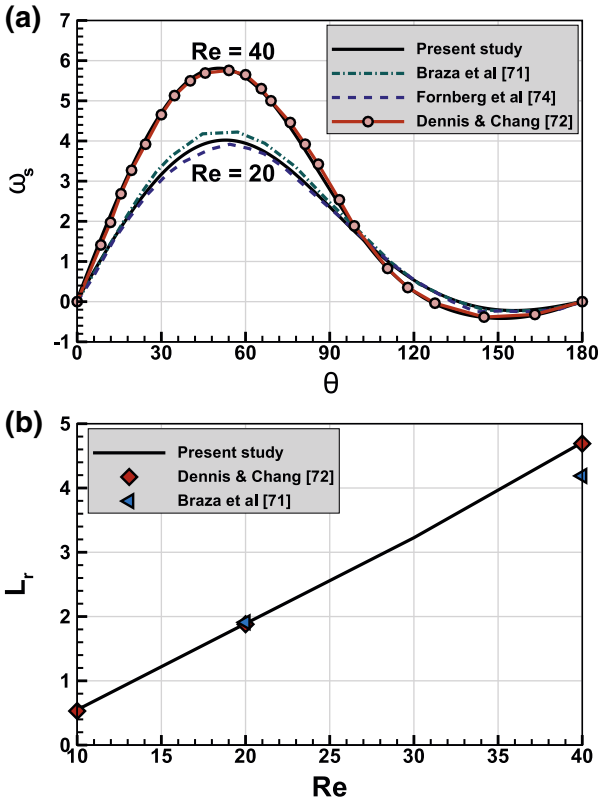

Fig. 4. Comparison of present code with literature for flow of pure fluid (water, $\phi = 0\%$) around a circular cylinder. (*a*) Distribution of wall vorticity along the cylinder surface at $Re = 20$, 40 and (*b*) variation of wake length at different Reynolds numbers ($10 \le Re \le 40$).

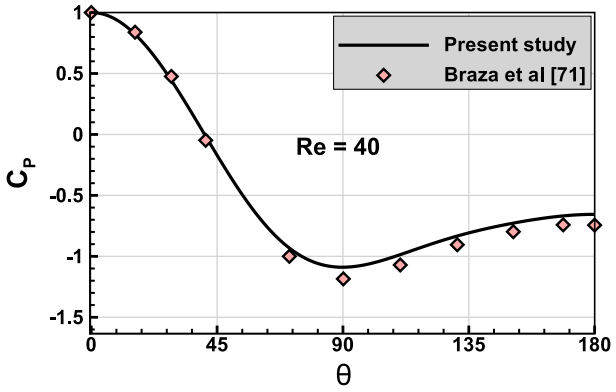

Fig. 5. Comparison of coefficient of pressure at $Re = 40$ from present code with literature for flow of pure fluid (water, $\phi = 0\%$) around a circular cylinder.

2.5.3. Mean Nusselt number (Nu_M)

The net heat transfer from the cylinder to the flowing nanofluid is represented and calculated by integrating the local Nusselt number along the surface of the cylinder and is given by

$$Nu_m = \frac{1}{\pi}\int_0^{\pi} Nu \sin\theta d\theta. \tag{19}$$

2.5.4. Enhancement in heat transfer (E)

In order to compare the heat transfer rates of pure fluid and nanofluids, the percentage enhancement in heat transfer is calculated

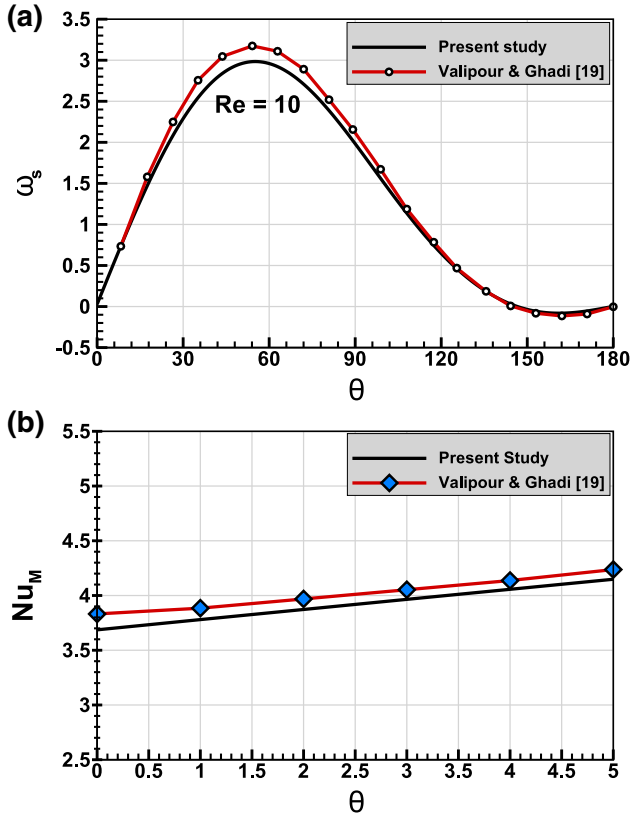

Fig. 6. Comparison of present code with literature data for Cu-water nanofluid flow around a circular cylinder at $Re = 10$. (*a*) Wall vorticity distribution along the cylinder surface with $\phi = 3\%$ and (*b*) variation of mean Nusselt number Nu_M with nanoparticle volume fraction ($0\% \le \phi \le 5\%$).

as follows:

$$E = \frac{Nu_M - Nu_{bf}}{Nu_{bf}} \times 100 \tag{20}$$

where, Nu_{bf} is the mean Nusselt number obtained using basefluid (pure water) and Nu_M is the mean Nusselt number at a specific volume fraction ϕ of nanofluid.

2.6. Numerical procedures and validation

2.6.1. Numerical methods

The governing equations of flow and heat transfer, which are non-linear partial differential equations are solved using a FORTRAN code based on Finite-Volume Method (FVM). A grid system of staggered nature is used where the velocity components are stored on cell faces while the scalar terms such as pressure and temperature are stored in the center of cells. SIMPLE algorithm has been utilized for the pressure-velocity coupling [67]. A third-order accurate QUICK scheme [68] has been employed to discretize the convective terms and the time derivatives are discretized using a first-order implicit scheme. Central difference scheme is used to discretize diffusion terms. A Tri-Diagonal Matrix Algorithm (TDMA) is used to iteratively solve the resulting system of discretized equations. The convergence of the iterative solution is checked by calculating the sum of the absolute differences of the solution variables between two successive iterations. Iterations are continued until the divergence criteria of 10^{-6} is achieved for all equations.

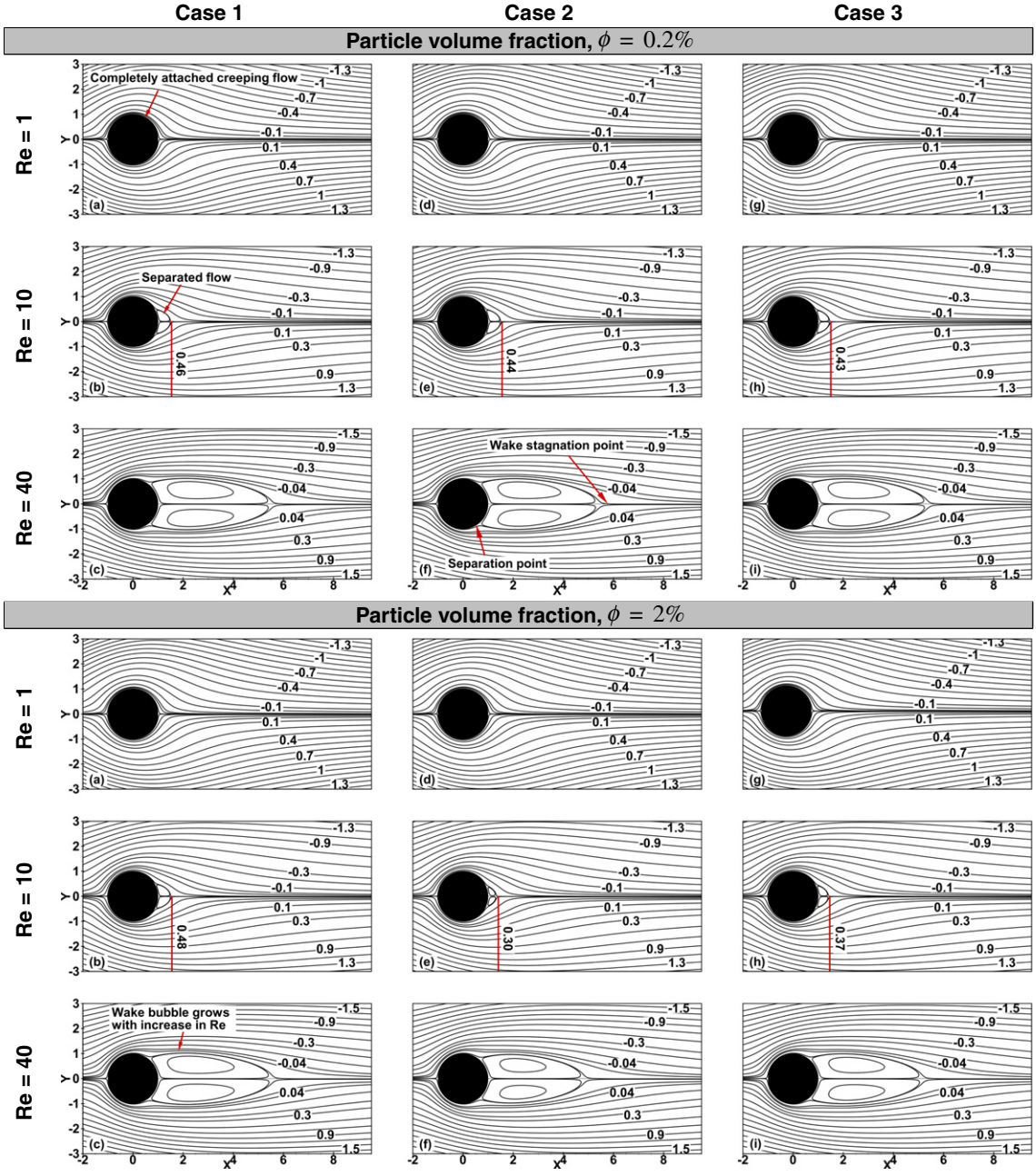

Fig. 7. Comparison of streamline patterns of forced convective flow of TiO_2-water nanofluid around a circular cylinder at Re = 1, 10 and 40, calculated using Basic models (Case 1), New models (Case 2) and Experimental data from [60] (Case 3) for effective thermal conductivity and viscosity at nanoparticle volume fractions ϕ = 0.2% and 2%. (Wake lengths are shown using vertical lines for easier comparison.)

2.7. Grid generation and independence test

The computational area is discretized into very small curvilinear elements with four nodes each. Multi-block technique using transfinite interpolation (algebraic method) method is used to generate the grid. The grid is further smoothed by a partial differential equation of elliptical type. The grid is more refined around the cylinder and little coarse away from the cylinder in far field (see Fig. 3). A systematic set of test runs have been conducted with different grid sizes ($m \times n$) and different outer boundary lengths (R_∞) to ensure that the obtained results are independent from the effects of grid. The different grid sizes and outer boundary lengths considered were analyzed with reference to the variation in coefficient of drag (C_D) and mean Nusselt number (Nu_M). This study which is done at $Re = 40$ is clearly presented in Table 3. The percentage differences in C_D and Nu_M for different grids and outer boundary lengths show that the grid 199×745 with outer boundary length ($R_\infty = 100$) will produce results independent of grid size with less computational expense.

2.7.1. Code validation

Numerical methodology used in this work is very common and used in many classical works available in literature to study the flow and heat transfer characteristics around a circular cylinder [69,70]. It is necessary to validate in order to dismiss the uncertainties involved in CFD codes. The validity of the physical model used in this work is proved by comparing our results for $Pr = 0.71$ with the standard literature of Braza et al. [71], Dennis & Chang [72] and Bhattacharya et al. [73]. It is seen from the Tables 4 and 5, that our results are within 3% variation from the results in literature. Parameters like wall vorticity (ω_s), wake length (L_r) and coefficient of pressure (C_p) for pure water ($\phi = 0\%$) at different

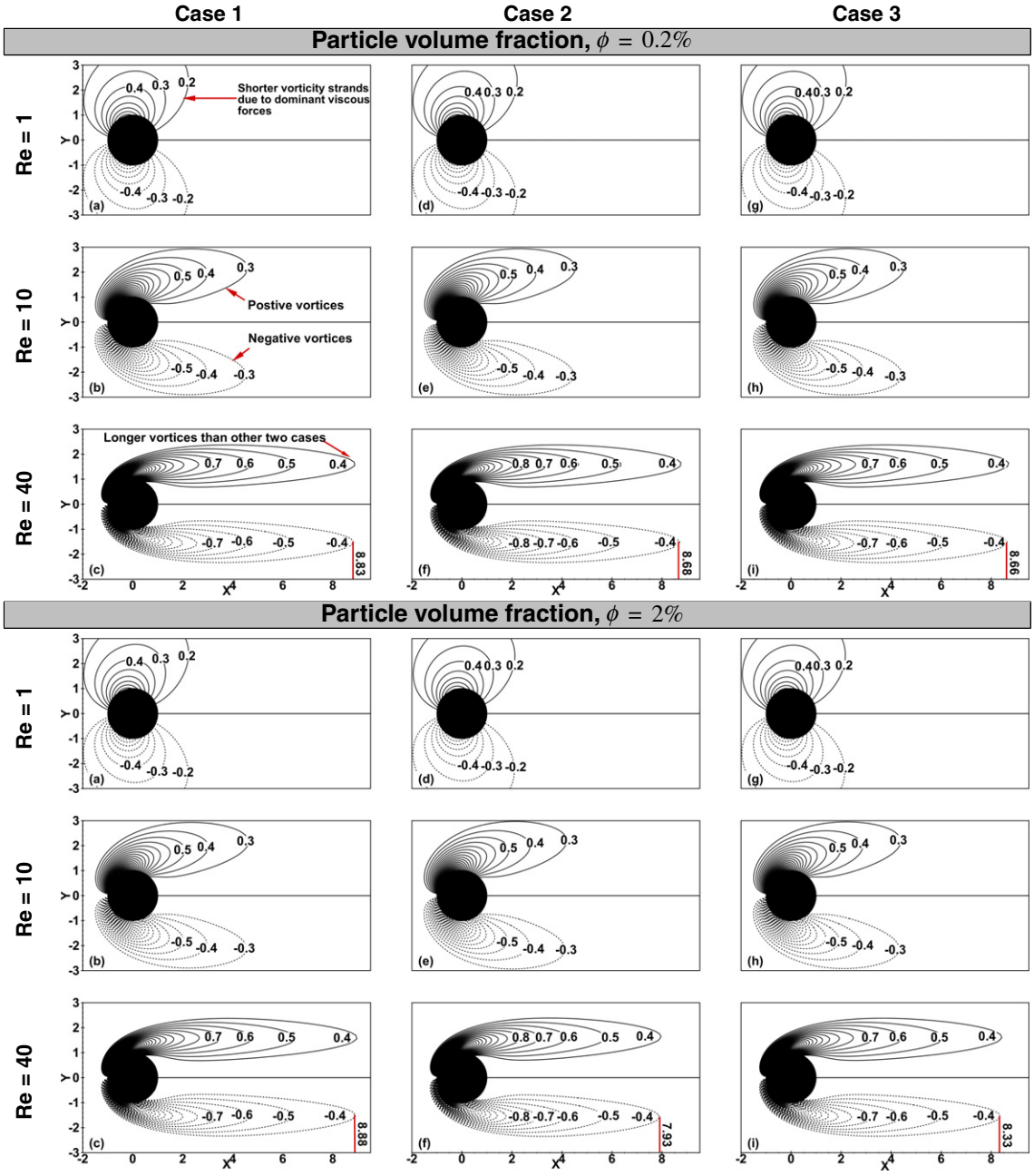

Fig. 8. Comparison of vorticity patterns of forced convective flow of TiO_2-water nanofluid around a circular cylinder at $Re = 1$, 10 and 40 calculated using Basic models (Case 1), New models (Case 2) and Experimental data from [60] (Case 3) for effective viscosity and thermal conductivity at nanoparticle volume fractions $\phi = 0.2\%$ and 2%. (Lengths of vorticity strands are shown using vertical lines for easier comparison.)

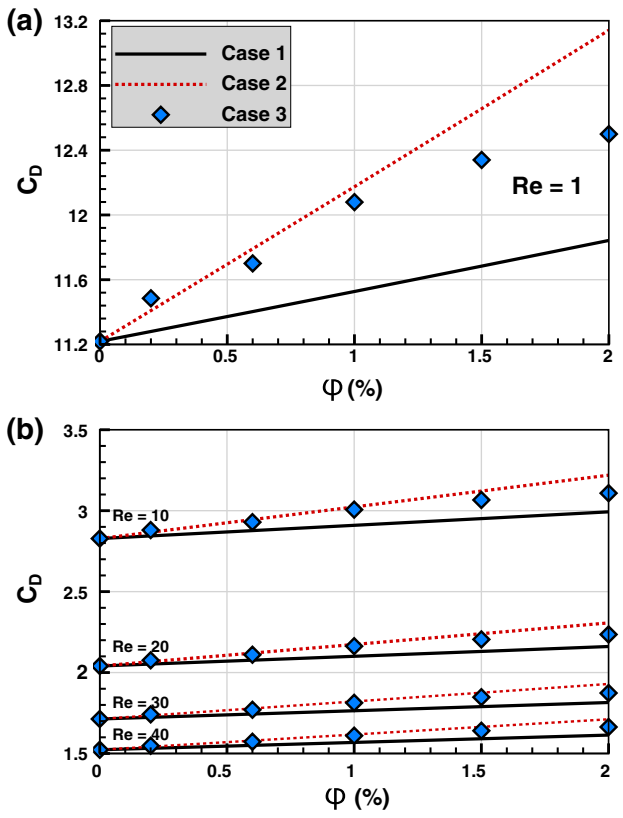

Fig. 9. Variation of coefficient of drag (C_D) with nanoparticle particle volume fractions ($0\% \le \phi \le 2\%$) of TiO_2-water nanofluid flowing around a circular cylinder calculated using Basic models (Case 1), New models (Case 2) and Experimental data from [60] (Case 3) for effective viscosity and thermal conductivity at (*a*) $Re = 1$ and (*b*) $10 \le Re \le 40$. Line legend in (*a*) is applicable for (*b*).

Reynolds numbers are compared with the available literature [71,72,74]. These comparisons are shown graphically in Figs. 4 and 5 and exhibit reliable coincidence. In addition to that, the results obtained for $\phi = 3\%$ using a copper-water nanofluid are also compared with the results of Valipour and Ghadi [19] (refer Fig. 6(*a*) and (*b*)). The variations observed are well within the limits and are acceptable. These minor variations can be due to differences in numerical methods, grid specifications and discretization schemes, etc. The comparison is agreeable and gives us confidence on the numerical results presented in this study.

3. Results and discussion

A complete numerical analysis of forced convective nanofluid flow and heat transfer around a circular cylinder is presented. All important flow and heat transfer characteristics are studied employing the following parameters.

Reynolds number: 1, 10 to 40 in steps of 10.

Nanofluid: TiO_2-water.

Particle volume fraction: 0%, 0.2%, 0.6%, 1%, 1.5% and 2%.

Particle diameter: 21 nm in Case 2.

Three cases (refer Section 2.4) are considered in this study. In each case, the effective thermal conductivity and viscosity of nanofluids are calculated as follows:

Case 1. Basic models (k_{eff} - MG model [57], μ_{eff} - Brinkman model [21]).

Case 2. New models (k_{eff} - Murugesan et al. [58], μ_{eff} - Chen et al. [59]).

Case 3. Experimental data by Duangthongsuk et al. [60].

A point by point comparative analysis of the three cases for calculating the effective properties is presented. This comparative study will help us to quantify the effects of uncertainties in effective properties on flow and heat transfer characteristics. The results are categorized into flow and heat transfer characteristics and are presented as follows:

3.1. Flow characteristics

A detailed discussion on variation of flow characteristics with particle volume fraction (ϕ), Reynolds number (Re) and the three cases of effective properties prediction is presented in this section.

3.1.1. Streamline patterns

Streamline patterns of nanofluid flow around a circular cylinder are presented in Fig. 7. For the purpose of brevity, streamline patterns at 0.2% and 2% particle volume fractions at Reynolds numbers $Re = 1, 10$ and 40 are alone presented. It can be clearly understood that, streamlines of flow are a function of Reynolds number and are also modified by addition of nanoparticles. At $Re = 1$, the flow is steady, laminar and is completely attached to the cylinder surface. This is because, at very low Reynolds numbers, the inertial forces are very weak and do not cause any flow separation. When Re is gradually increased, at $Re = 10$, the flow is unable to adhere to the cylinder surface in the downstream region and as a result of this, flow separation takes place and a recirculation/wake bubble is formed from the trailing edge of the cylinder. When the Reynolds number is further increased, the length of the recirculating wake bubble gradually increases and it is maximum at $Re = 40$. The effect of particle volume fraction is different in each case considered in this work. In Case 1, increase in particle volume fraction leads to an accelerated flow, which is understood from the increase in wake length with increase in ϕ. Whereas in Case 2 and Case 3, the wake length decreases with increase in particle volume fraction. This indicates that addition of nanoparticles causes a deceleration in flow in

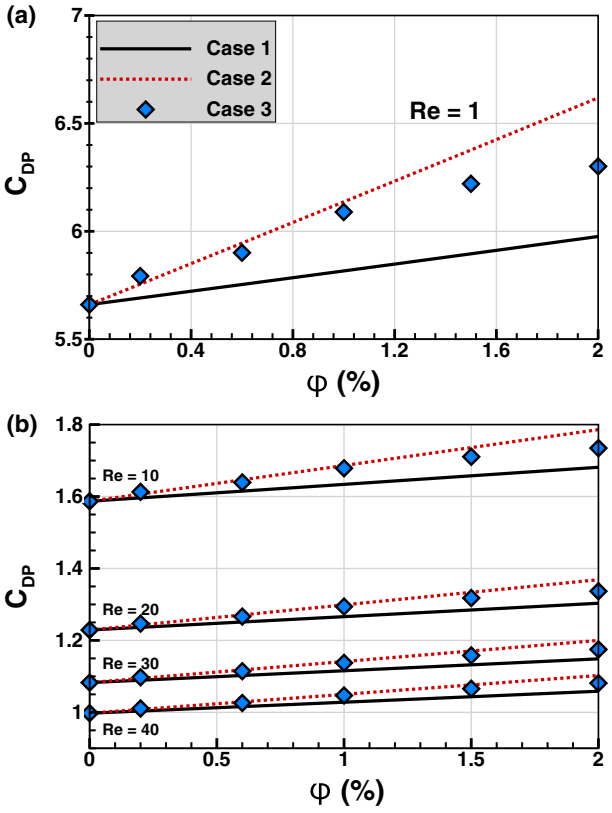

Fig. 10. Variation of coefficient of drag due to pressure forces (C_{DP}) with nanoparticle particle volume fractions ($0\% \le \phi \le 2\%$) of TiO_2-water nanofluid flowing around a circular cylinder calculated using Basic models (Case 1), New models (Case 2) and Experimental data from [60] (Case 3) for effective viscosity and thermal conductivity at (*a*) $Re = 1$ and (*b*) $10 \le Re \le 40$. Line legend in (*a*) is applicable for (*b*).

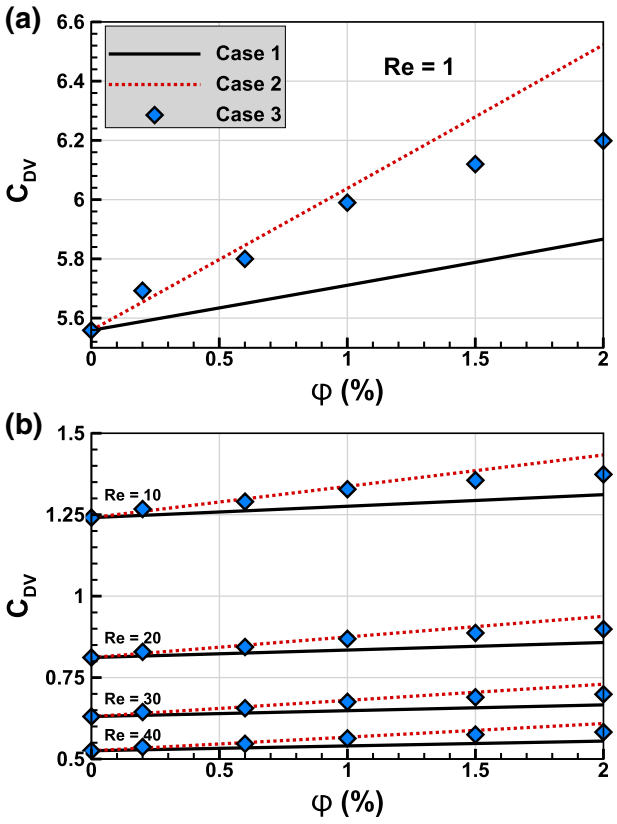

Fig. 11. Variation of coefficient of drag due to viscous forces (C_{DV}) with nanoparticle particle volume fractions ($0\% \le \phi \le 2\%$) of TiO_2-water nanofluid flowing around a circular cylinder calculated using Basic models (Case 1), New models (Case 2) and Experimental data from [60] (Case 3) for effective viscosity and thermal conductivity at (*a*) $Re = 1$ and (*b*) $10 \le Re \le 40$. Line legend in (*a*) is applicable for (*b*).

Case 2 and Case 3. This is qualitatively a completely contradicting phenomenon from Case 1. Even though Case 2 and Case 3 show a decelerated flow, they differ quantitatively. This can be understood from the wake lengths shown using a vertical line to aid the readers.

3.1.2. Vorticity patterns

Vorticity pattern around a circular cylinder during a steady forced convective nanofluid flow is shown in Fig. 8. Positive vortices are shown in solid lines and the negative vortices are shown in dotted lines. Similar to the streamline patterns, vorticity patterns are also a function of Reynolds number and particle volume fraction. Firstly, we explain the effect of increase in Reynolds number. At $Re = 1$, the flow velocity is very less and the effect of inertial forces is weak. Viscous forces are very dominant in this range of Reynolds number and restrict the movement of fluid. Hence, the vortices are weaker and short in length. With further increase in Reynolds number, the length of vorticity strands gets longer indicating a growth in strength of vorticity. This is due to the increase in inertial forces with increase in flow velocity or the Reynolds number. At $Re = 40$, the vorticity strands are much longer indicating stronger vorticity due to stronger inertial forces. This phenomenon of increase in vorticity strength with increase in Reynolds number is apparently visible in the plots presented. Coming to effect of particle volume fraction, vorticity patterns differ both qualitatively and quantitatively between each case. In Case 1, the strength of the vorticity increases with increase in particle volume fraction. This can be inferred by the longer vorticity strands at $\phi = 2\%$ than at $\phi = 0.2\%$. Length of the vorticity strands are indicated by vertical lines for the comfort of readers. As already explained, this shows the accelerated flow with increase in particle volume fraction in Case 1. Whereas in Cases 2 and 3, the flow is decelerated by the addition of nanoparticles. This causes a decrease in length of vorticity strands, (i.e.,) weaker vortices in Case 2 and Case 3. From this, we can understand that Case 1 shows a trend completely different from Case 2 and Case 3. Even though Case 2 and Case 3 show the same trend, their numerical values differ from each other.

3.1.3. Coefficients of drag (C_D, C_{DV}, C_{DP})

Drag coefficients are calculated by Eqs. (15) to (17). Variations of coefficients of drag (C_D, C_{DP} and C_{DV}) with particle volume fraction ϕ and at $1 \le Re \le 40$ are presented in Figs. 9 to 11. Drag coefficients are influenced by the Reynolds number of the flow. At $Re = 1$, due to dominant viscous forces and thick viscous region, very high C_D, C_{DV} and C_{DP} are seen. When the Reynolds number is increased to 10, there is a sudden drop in drag coefficients due to decrease in thickness of the viscous layer. With further increase in *Re*, corresponding decrease in C_D, C_{DP}

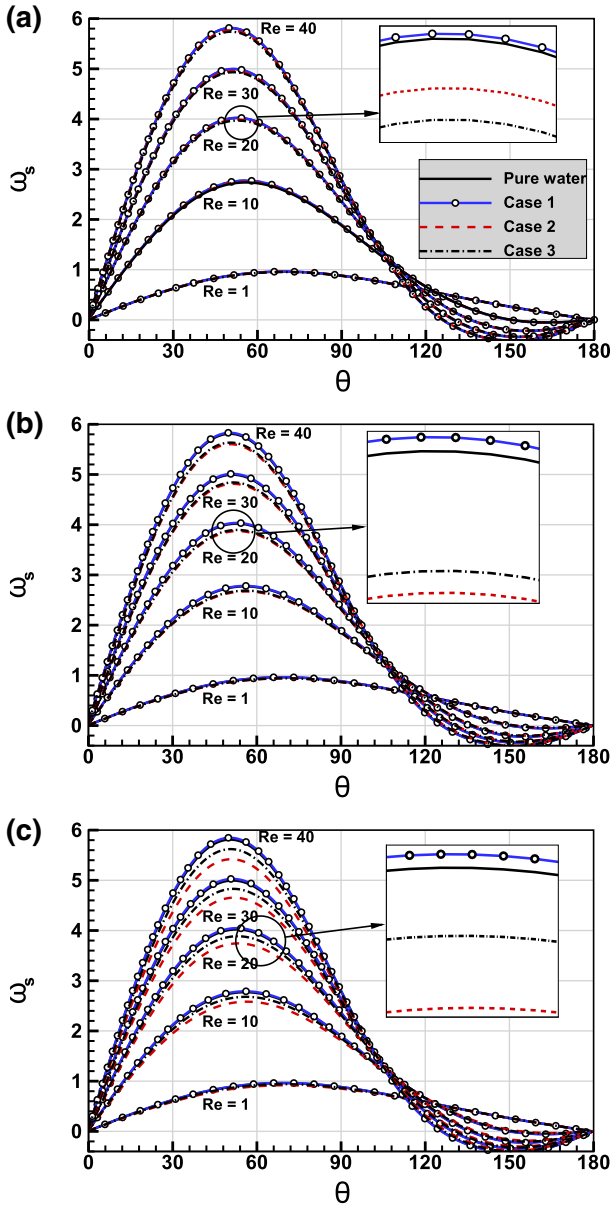

Fig. 12. Distribution of wall vorticity ω_s along the cylinder surface for TiO_2-water nanofluid flow calculated using Basic models (Case 1), New models (Case 2) and Experimental data from [60] (Case 3) for effective thermal conductivity and viscosity at different Reynolds numbers $1 \le Re \le 40$ for (*a*) $\phi = 0.2\%$, (*b*) $\phi = 1\%$ and (*c*) $\phi = 2\%$. Line legend in (*a*) is applicable for (*b*) and (*c*).

and C_{DV} are noted. Irrespective of the Reynolds number, coefficients of drag (C_D, C_{DP} and C_{DV}) increase with increase in particle volume fraction. This is because of the increase in viscosity caused due to addition of nanoparticles. This effect is different in each case. The basic Brinkman model in Case 1 under predicts the C_D, C_{DV} and C_{DP} compared to other two cases. Whereas, an over prediction is done by the correlation used in Case 2. Thus, we see highest level of coefficients of drag (C_D, C_{DP} and C_{DV}) in Case 2; while, the lowest level is seen in Case 1. Even though, Case 3 which considers the experimental data for effective viscosity lies intermediate to Case 1 and Case 2, its values are closer to Case 2. This variation is clearly seen in Fig. 9(a), Fig. 10(a) and Fig. 11(a). Variation between each case is high at higher volume fractions. This uncertainty in viscosity prediction by the models is much magnified at lower Reynolds number due to thicker viscous region. At $Re = 1$ and $\phi = 2\%$, there is 5.5% variation between Case 1 and Case 3, 4.8% variation between Case 2 and Case 3 and 10.9% variation between Cases 1 and 2.

3.1.4. Distribution of surface vorticity (ω_s)

The distribution of vorticity along the cylinder surface is presented in Fig. 12(a), (b) and (c). For the purpose of brevity the plots at 0.2%, 1% and 2% volume fractions are alone presented. At the front stagnation point, the surface vorticity is zero and gradually starts increasing along the cylinder surface. It reaches a maximum value and again decreases in the downstream region to attain a negative value in the recirculation region. After showing negative vorticity in the recirculation region, a marginal increase is observed near the rear stagnation point to reach zero vorticity. The vorticity along the cylinder surface is dependent on Re. At $Re = 1$, due to dominant viscous forces; resistance to the motion of fluid will be high. Hence, a weaker vorticity distribution along the cylinder surface is noticed. When Re is increased from 10 to 40, the inertial forces become more dominant, promote rotary motion of the fluid; thereby leading to an increase in vorticity distribution. It is clearly evident from the plots that the vorticity distribution along the cylinder surface increases with increase in Reynolds number. Variation in vorticity distribution at different particle volume fractions are very less. It is more or less in the same range for $\phi = 0.2\%$, 1% and 2%. The variations between each cases are lower at smaller volume fractions (see Fig. 12(a)). When the volume fraction increases, the effects of models are clearly seen at $Re = 10, 20, 30$ and 40. Whereas at $Re = 1$, influence of models is weak. In Fig. 12(c), a clear variation is visible between three cases at higher Re. In the zoomed views presented in Fig. 12(a), (b) and (c), we can see that Case 1 shows stronger vorticity than the pure fluid. But, this is completely different in Case 2 and Case 3; where the vorticity distribution of nanofluid is weaker than that of the pure fluid. Thus, we understand that the flow is accelerated by addition of nanoparticles in Case 1; but in Case 2 and Case 3, flow is decelerated by the addition of nanoparticles.

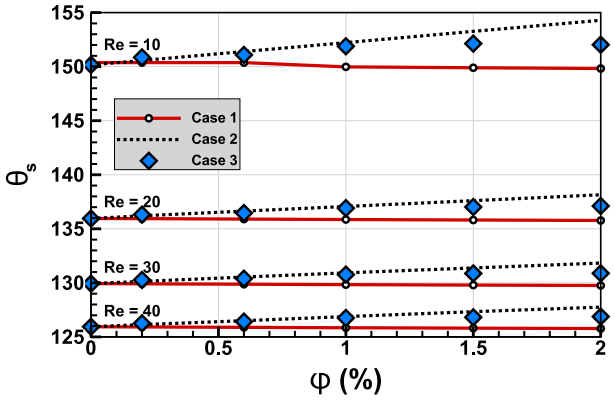

Fig. 14. Variation of separation angle (θ_s) at different nanoparticle volume fractions ($0\% \le \phi \le 2\%$) of TiO_2-water nanofluid flow around a circular cylinder at $Re = 10$ to 40, calculated using Basic models (Case 1), New models (Case 2) and Experimental data from [60] (Case 3) for effective thermal conductivity and viscosity.

3.1.5. Wake length (L_r)

Already in Section 3.1.1, by observing the streamline patterns, we know that flow is completely attached at to the cylinder surface at $Re = 1$ and at $Re = 10$ due to increase in inertial forces, flow is detached from the cylinder surface and forms a recirculating wake bubble in the downstream side of cylinder. Length of this bubble from the cylinder surface to the wake stagnation point is known as the wake length. With further increase in Reynolds number, wake length increases gradually and reaches the maximum value at $Re = 40$. This phenomenon is neatly presented in Fig. 13. Wake length is also influenced by the addition of nanoparticles. In Case 1, we see a marginal increase in wake length by increasing the particle volume fraction. This means that the flow separation is promoted by adding nanoparticles in Case 1. Whereas in Case 2 and Case 3, we see that the wake length decreases significantly with addition of nanoparticles. This is because of the higher increase in viscosity with increase in particle volume fraction. This increase in viscosity restricts the flow separation and results in shorter wake lengths. Thus, we see a completely contradicting behavior in Case 1 when compared to the other two cases. The variation between three cases are very high at higher Reynolds numbers and volume fractions. At $Re = 40$ and $\phi = 2\%$, there is a 9.3% variation between Case 1 and Case 3, 7.8% variation between Case 2 and Case 3 while Case 1 and Case 2 vary by 15.9%.

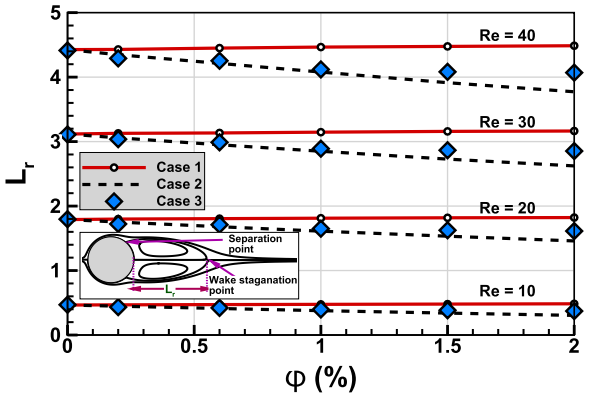

Fig. 13. Variation of wake length L_r at different nanoparticle volume fractions ($0\% \le \phi \le 2\%$) of TiO_2-water nanofluid flow around a circular cylinder at $Re = 10$ to 40, calculated using Basic models (Case 1), New models (Case 2) and Experimental data from [60] (Case 3) for effective thermal conductivity and viscosity.

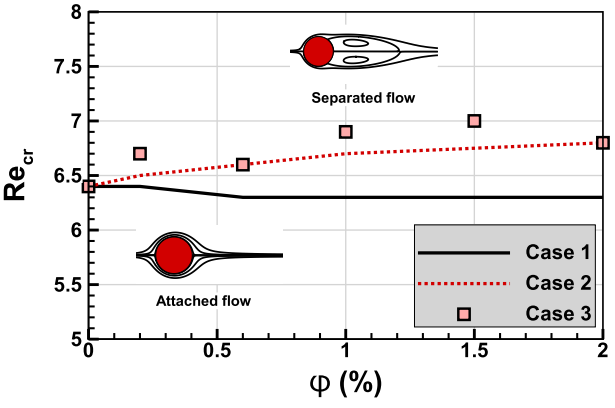

Fig. 15. Onset of flow separation at different nanoparticle volume fractions ($0\% \le \phi \le 2\%$) of TiO_2-water nanofluid flow around a circular cylinder, calculated using Basic models (Case 1), New models (Case 2) and Experimental data from [60] (Case 3) for effective thermal conductivity and viscosity.

3.1.6. Separation angle (θ_s)

At higher Reynolds numbers, the flow is separated from the surface of the cylinder on the downstream side. The point or angle at which the flow separation takes place is known as the separation angle. Influence of *Re* and ϕ on separation angle is shown in Fig. 14. Increase in Reynolds number causes the flow to separate earlier along the cylinder surface. This can be attributed to the increase in inertial forces at higher Reynolds numbers. This separation angle is also a function of particle volume fraction. In Case 1, the separation angle decreases with increase in particle volume fraction. This indicates the promotion of flow separation by adding nanoparticles. A completely new phenomenon is seen in Case 2 and Case 3, where we observe an increase in separation angle with the addition of nanoparticles. This shows that the flow separation is delayed by the addition of nanoparticles. This is because of the sharp increase in viscosity in Case 2 and Case 3, which makes the flow to be attached to the cylinder surface for a longer duration. At $Re = 10$ and $\phi = 2\%$, there is 1.4% variation between Case 1 and Case 3, 1.5% variation between Case 2 and Case 3 and 2.9% variation between Case 1 and Case 2.

3.1.7. Critical Reynolds number (Re_{cr})

The Reynolds number at which the flow separation is first witnessed at a particular particle volume fraction is defined as the critical Reynolds number (Re_{cr}). The Reynolds number at which flow separation is first cited varies for each particle volume fraction (see Fig. 15). In the region above the curve, the flow is separated and a recirculation/wake bubble on the downstream side of the cylinder is formed. Whereas, in the region below the curve the flow is completely attached and creeping over the cylinder surface. The variation in critical Reynolds number is

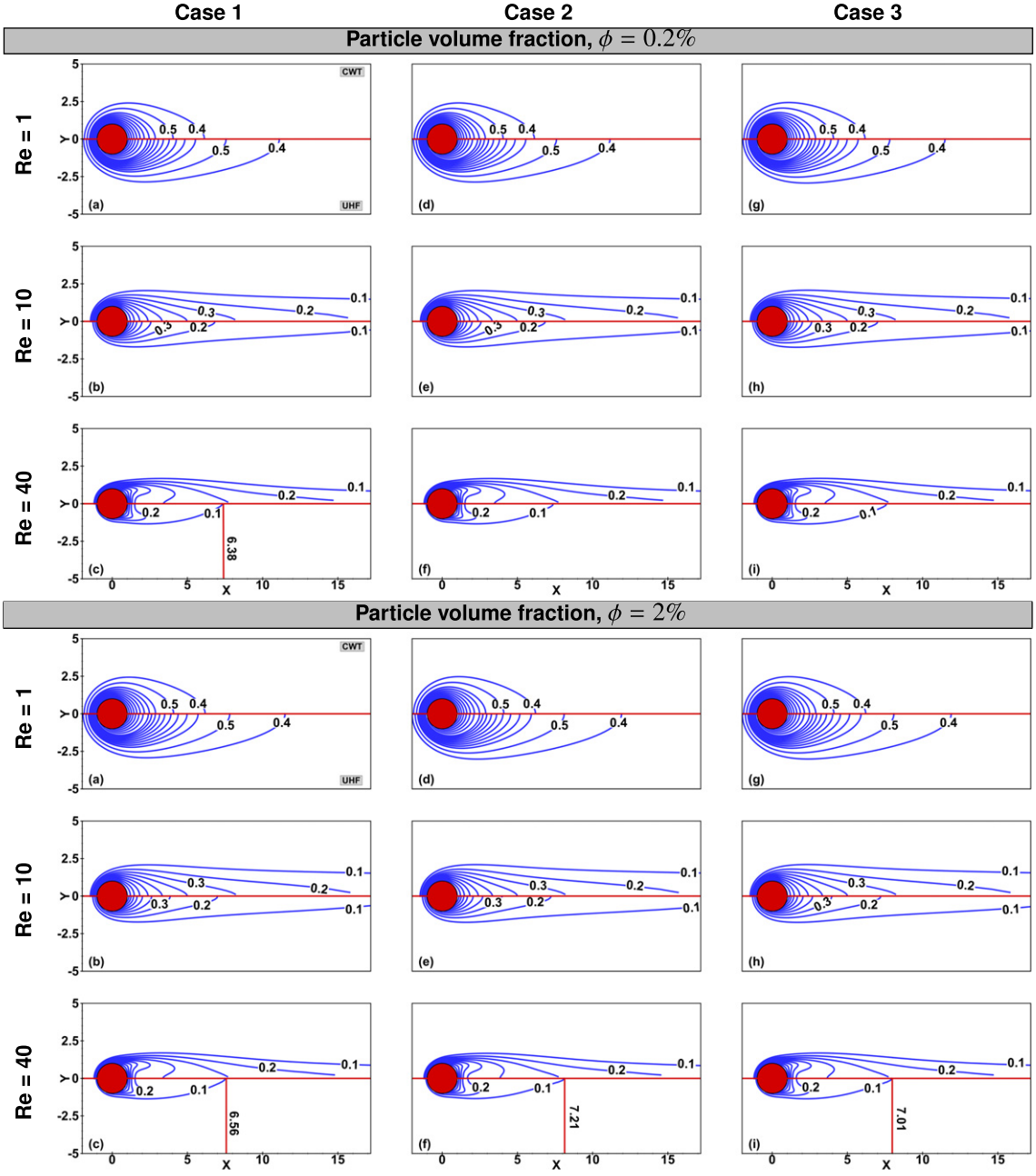

Fig. 16. Comparison of isotherm patterns of forced convective flow of TiO_2-water nanofluid around a circular cylinder at $Re = 1$, 10 and 40, calculated using Basic models (Case 1), New models (Case 2) and Experimental data from [60] (Case 3) for effective thermal conductivity and viscosity with Uniform Heat Flux (UHF) and Constant Wall Temperature conditions applied on the cylinder surface at nanoparticle volume fractions $\phi = 0.2\%$ and 2%. (Lengths of isotherms are shown using vertical lines. Upper half represents CWT condition and lower half denotes UHF condition.)

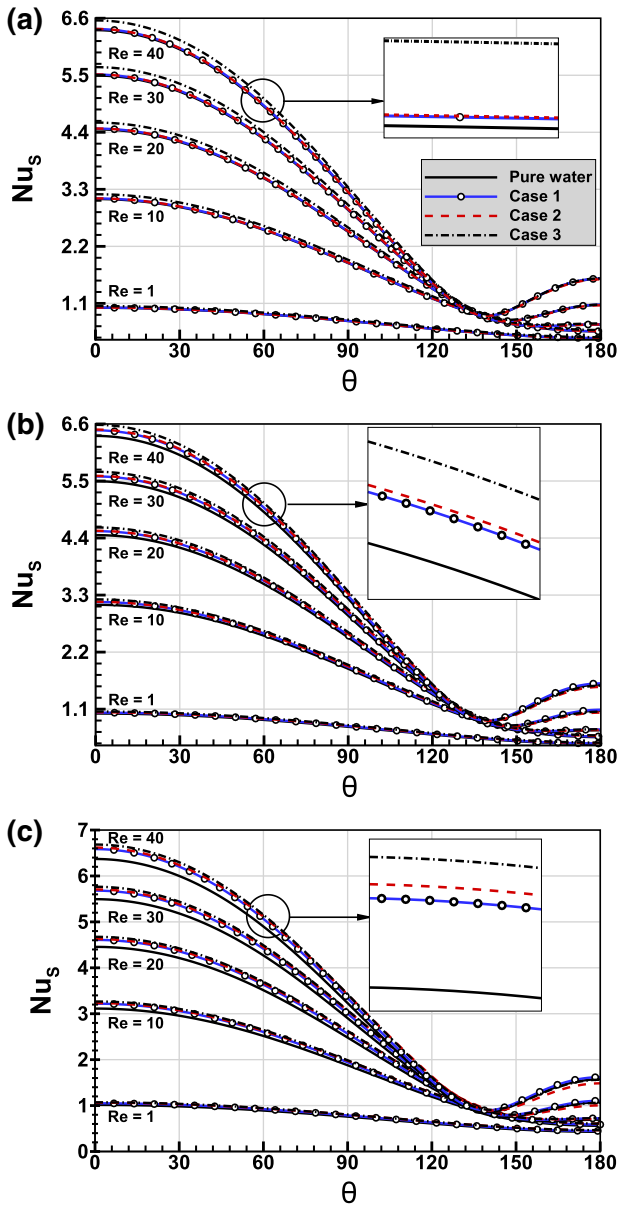

Fig. 17. Distribution of local Nusselt number along the cylinder surface Nu_S for TiO_2-water nanofluid flow around a circular cylinder at $1 \le Re \le 40$, calculated using Basic models (Case 1), New models (Case 2) and Experimental data from [60] (Case 3) for effective thermal conductivity and viscosity with Constant Wall Temperature (CWT) condition applied on the cylinder surface at (*a*) $\phi = 0.2\%$, (*b*) $\phi = 1\%$ and (*c*) $\phi = 2\%$. Line legend in (*a*) is applicable for (*b*) and (*c*).

different for each case. Case 1, which considers the basic Brinkman model shows no significant change in Re_{cr} with increase in particle volume fraction. After a slight decrease, the curve is almost constant for Case 1. Whereas, Case 2 which considers a correlation by Chen et al. [59], shows a steady marginal increase. A similar trend is seen in Case 3 in which the experimental data from [60] for effective viscosity and thermal conductivity are considered. The values of Re_{cr} are highest for Case 3, lowest for Case 1 and Case 2 lies intermediate to them.

3.2. Heat transfer characteristics

Heat transfer characteristics are a function of particle volume fraction (ϕ), Reynolds number (Re) and the boundary condition applied on the cylinder surface. Apart from these parameters, the variations due to uncertainties in effective property models considered in three cases are also clearly highlighted in this section.

3.2.1. Isotherm patterns

Isotherms are imaginary lines of constant temperature which show the temperature distribution in the flow region. Isotherm patterns at $\phi = 0.2\%$ and $\phi = 2\%$ and at $Re = 1$, 10 and 40 are shown in Fig. 16. The temperature field around the cylinder is affected by the Reynolds number, particle volume fraction and the temperature boundary condition (The upper half represents CWT and the lower half of the figure represent UHF condition). As the flow considered in this study is in laminar steady flow regime, we notice that the isotherms are steady and symmetric about the horizontal axis. The maximum heat transfer is noticed at the front stagnation point which is clearly understood by the increased clustering of isotherms. As we move along the downstream region, we observe that the isotherms are sparsely spaced. With increase in Reynolds number, the isotherms become slightly closer in the downstream region due to increase in the flow recirculation. The thumb like projection seen in the isotherms is more defined and sharp at $Re = 40$.

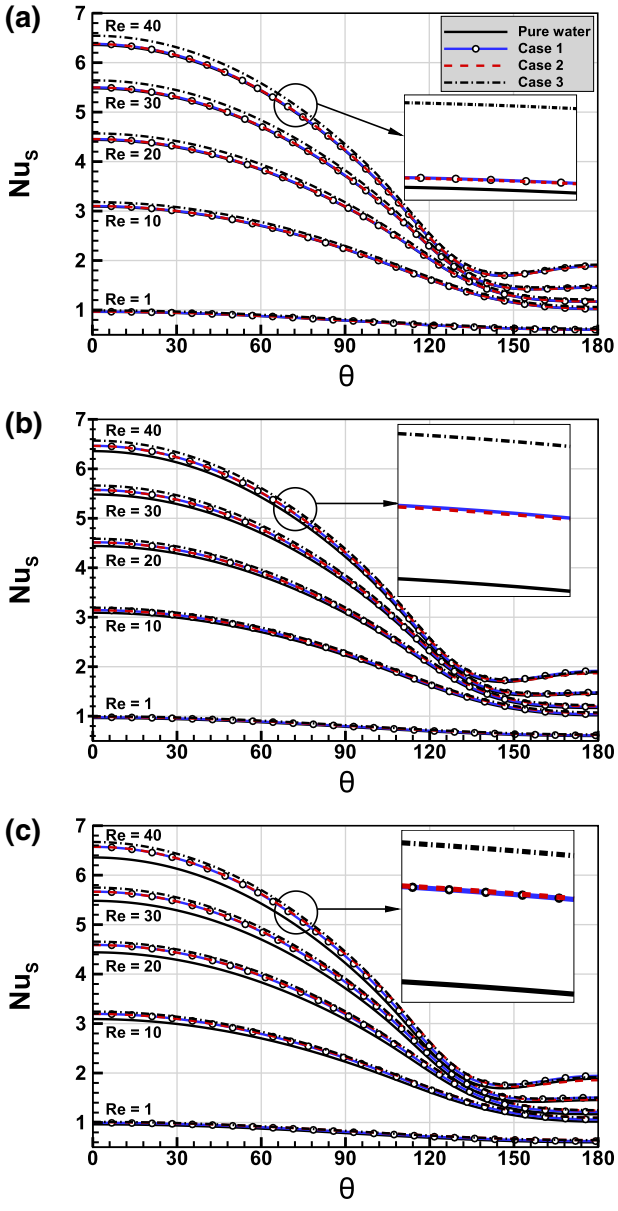

Fig. 18. Distribution of local Nusselt number along the cylinder surface Nu_S for TiO_2-water nanofluid flow around a circular cylinder at $1 \le Re \le 40$, calculated using Basic models (Case 1), New models (Case 2) and Experimental data from [60] (Case 3) for effective thermal conductivity and viscosity with Uniform Heat Flux (UHF) condition applied on the cylinder surface at (*a*) $\phi = 0.2\%$, (*b*) $\phi = 1\%$ and (*c*) $\phi = 2\%$. Line legend in (*a*) is applicable for (*b*) and (*c*).

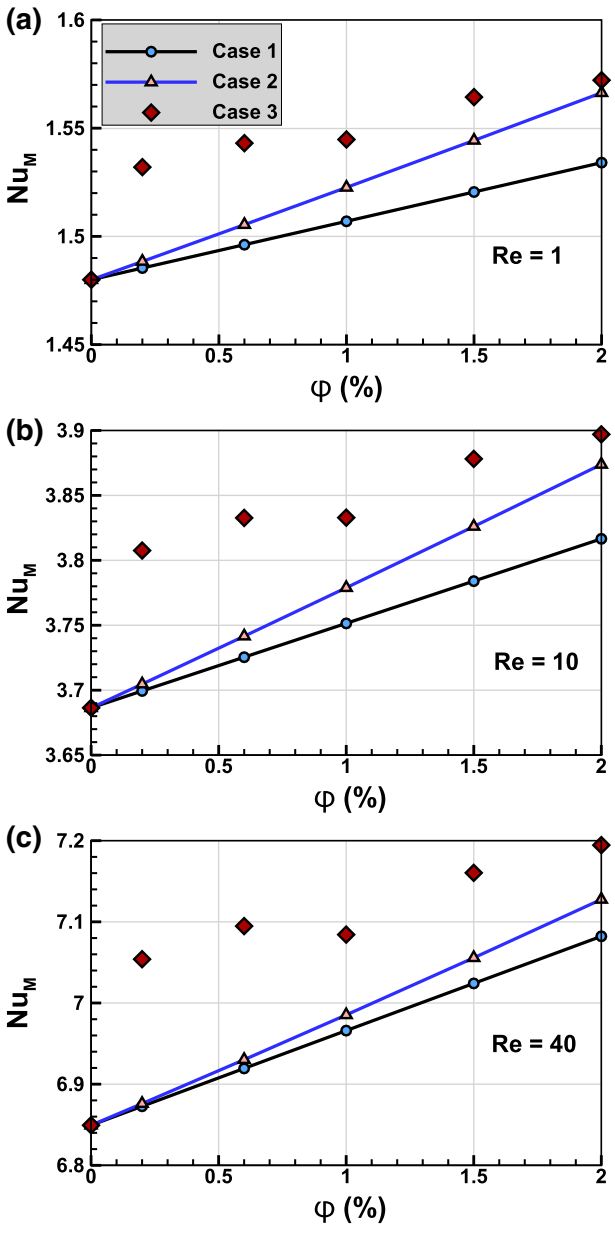

Fig. 19. Variation of mean Nusselt number Nu_M for TiO_2-water nanofluid flow around a circular cylinder at different nanoparticle volume fractions ($0\% \le \phi \le 2\%$), calculated using Basic models (Case 1), New models (Case 2) and Experimental data from [60] (Case 3) for effective thermal conductivity and viscosity with Constant Wall Temperature (CWT) condition applied on the cylinder surface at (*a*) $Re = 1$, (*b*) $Re = 10$ and (*c*) $Re = 40$. Line legend in (*a*) is applicable for (*b*) and (*c*).

At $Re = 1$, due to the thick boundary layer and absence of flow separation, the temperature difference in UHF condition is much higher than CWT condition. Hence, the isotherms are closer in CWT condition than UHF condition. At $Re > 10$, the boundary layer becomes thin. In this condition, the temperature difference in UHF boundary condition is higher. This causes comparably higher heat transport in UHF condition than in CWT boundary condition, which leads to closer isotherms in UHF than CWT. Addition of nanoparticles did not cause any significant variation in the isotherm patterns. There is no much significant variations among the three cases. Considering the very small variations, we can say that the spacing of isotherms are almost same in all three cases.

3.2.2. Distribution of local Nusselt number (Nu_s)

The distribution of local Nusselt number along the cylinder surface is presented in Figs. 17 and 18. For the purpose of brevity, we have only presented the local Nusselt number distribution at $\phi = 0.2\%$, 1% and 2%. It can be clearly seen that the local Nusselt number is a strong function of *Re*. As *Re* is increased from 1 to 40, the Nusselt number distribution increases remarkably. The local Nusselt number values also vary along the surface of cylinder. The local Nusselt number is maximum in the upstream side on the front stagnation point and then it gradually decreases and reaches the lowest value near the flow separation point. Again a slight increase is observed in the recirculation region. Nu_s distribution also varies with the boundary condition. In general, we can say UHF condition shows higher values of local Nusselt number distribution. The local Nusselt number distribution of nanofluids are higher than that of the pure fluid due to their enhanced thermal conductivities. Nusselt number values increase with increase in particle volume fraction. Case 1 which uses the basic MG model predicts lower values of Nu_s than other two cases. Case 2, which considers a Brownian motion

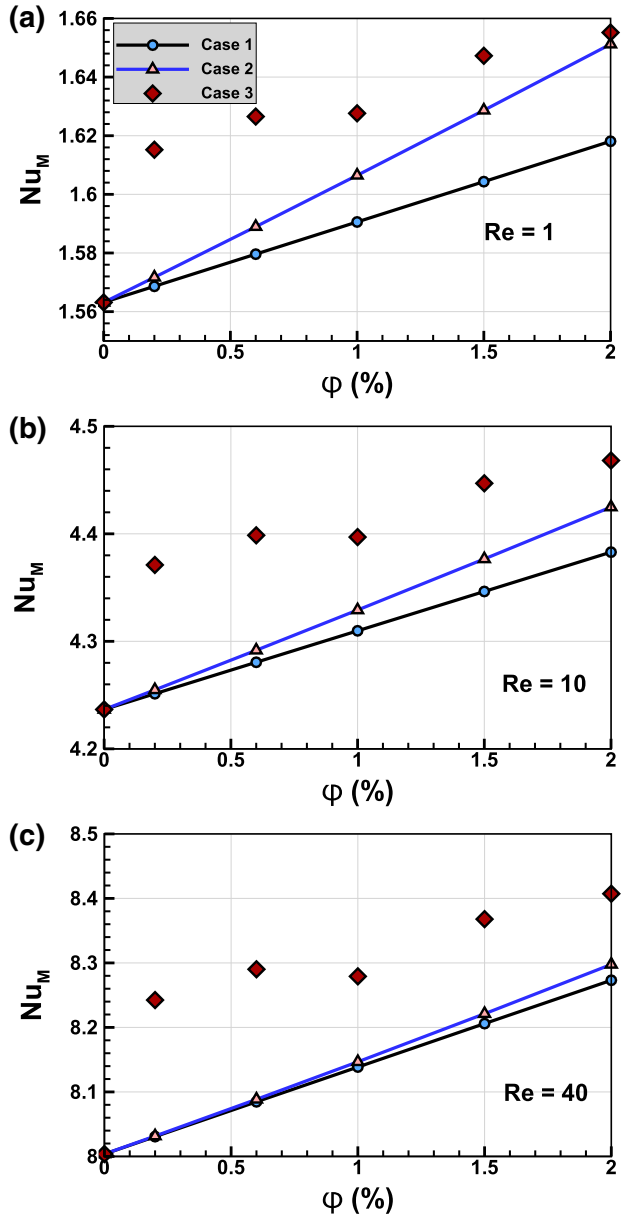

Fig. 20. Variation of mean Nusselt number Nu_M for TiO_2-water nanofluid flow around a circular cylinder at different nanoparticle volume fractions ($0\% \le \phi \le 2\%$), calculated using Basic models (Case 3), New models (Case 2) and Experimental data from [60] (Case 3) for effective viscosity and thermal conductivity with Uniform Heat Flux (UHF) condition applied on the cylinder surface at (*a*) $Re = 1$, (*b*) $Re = 10$ and (*c*) $Re = 40$. Line legend in (*a*) is applicable for (*b*) and (*c*).

and interfacial layer based model predicts a slightly higher value. But, Case 3 which uses the experimental data from [60] for effective viscosity and thermal conductivity shows higher values than the other two cases. This indicates that none of the models are capable to give a precise prediction. Moreover, this variation between three cases is augmented at higher values of *Re* and ϕ.

3.2.3. Mean Nusselt number (Nu_M)

The variation of mean Nusselt number in constant wall temperature and uniform heat flux condition have been presented in Figs. 19 and 20. Mean Nusselt number is a strong function of *Re*. With increase in *Re*, we see a significant increase in Nu_M. The mean Nusselt number (Nu_M) is lowest for $Re = 1$ and the highest value is seen at $Re = 40$ for both CWT and UHF conditions. The Nu_M values are higher for uniform heat flux boundary condition than the constant wall temperature condition. Adding to that, we can see that Nu_M increases with addition of nanoparticles. In both the boundary conditions, Nu_M is higher at higher particle volume fractions. The Nu_M increases linearly with increase in particle volume fraction. This is because of the enhanced thermal conductivities of nanofluids. Comparing the three cases, Case 3 which takes into account experimental data from [60] for effective viscosity and thermal conductivity shows highest values of Nu_M in both UHF and CWT conditions and also at all values of *Re*. In Case 2, as we consider a Brownian motion and interfacial layer based model, we see slightly enhanced heat transfer than Case 1 which considers a classical EMT based model. But, Case 3 values are significantly higher than other two cases at all Reynolds numbers and volume fractions. This shows that both the models are under predicting the thermal conductivity, when compared to experimental data taken into account.

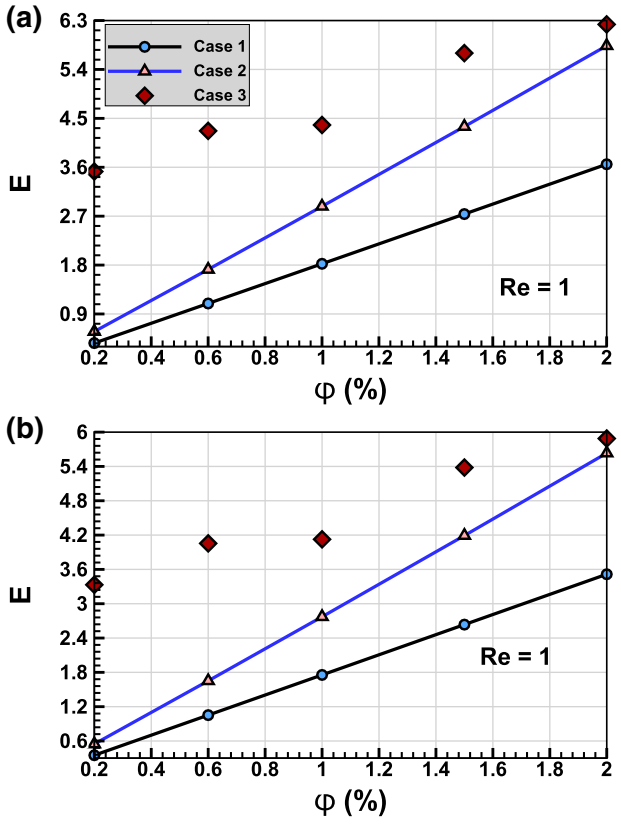

Fig. 21. Enhancement in heat transfer at different nanoparticle volume fractions ($0\% \le \phi \le 2\%$) of TiO_2-water nanofluid flow around a circular cylinder at $Re = 1$, calculated using Basic models (Case 1), New models (Case 2) and Experimental data from [60] (Case 3) for effective viscosity and thermal conductivity with (*a*) CWT condition and (*b*) UHF condition on the cylinder surface. Line legend in (*a*) is applicable for (*b*).

3.2.4. Heat transfer enhancement (E)

The percentage enhancement in heat transfer using nanofluids at CWT and UHF boundary conditions are presented in Fig. 21(*a*) and (*b*). It is seen that the percentage enhancement is almost same for all values of *Re*. Thus, for the purpose of brevity we present only the percentage enhancement at $Re = 1$. But, the heat transfer enhancement show a strong dependence on particle volume fraction. It is seen that the percentage enhancement in heat transfer increases linearly with increase in particle volume fraction. Case 1 in which the basic MG model is used, shows the lowest values of enhancement. Case 2 which uses a Brownian motion and interfacial layer based model produces higher enhancement than the Case 1. The difference between Case 1 and Case 2 is higher at higher particle volume fractions. Case 3 in which the experimental data from [60] for effective viscosity and thermal conductivity are employed shows very high values than the other two cases. At $Re = 1$, $\phi = 2\%$ and using CWT condition; heat transfer enhancement in Case 1 and Case 3 varies by 70.4%. Between Case 2 and Case 3 67.3% variation is seen; while, Case 1 and Case 2 vary by 59.6%. Thus, the model values of Case 1 and Case 2 are much lower than the Case 3, showing the inability of both the models to match with the experimental data taken into account.

4. Concluding remarks

A 2-D steady forced convective nanofluid flow around a circular cylinder has been investigated. Flow and heat transfer characteristics are studied using both CWT and UHF boundary conditions. Salient feature of this work is that, apart from analyzing the effects of particle volume fraction and Reynolds number; a comparative study using three cases in which different models for effective viscosity and thermal conductivity and experimental data available in literature were used. The results of the comparative analysis can be summarized as follows:

- The basic model by Brinkman [21] to predict the effective viscosity of nanofluids used in Case 1 indicates an accelerated flow with increase in particle volume fraction which leads to earlier flow separation, longer wake lengths and stronger vortices.
- A completely new and unique phenomenon is seen in Case 2. The recent correlation for effective viscosity of nanofluids by Chen et al. [59] used in Case 2 exhibits an decelerated flow which shows delayed flow separation, shorter wake lengths and weak vortices.
- Thus, Case 1 and Case 2 show completely contradicting phenomena. This is because the basic Brinkman model in Case 1 shows only a marginal increase in dynamic viscosity with increase in particle volume fraction. This leads to decrease in kinematic viscosity with increase in particle volume fraction. We all know that a decrease in kinematic viscosity will lead to an accelerated flow.
- But, the correlation used in Case 2 captures the increase in viscosity due to increase in particle volume fraction quite well than the Brinkman model. Hence, in Case 2 we observe an increase in kinematic viscosity which leads to a decelerated flow.
- Case 3 shows similar trend as that of Case 2. Even though Cases 2 and 3 show similar trends in flow characteristics, they vary quantitatively. Thus, models used in both the cases are not precise enough to match with the experimental data of effective viscosity and thermal conductivity considered in Case 3.
- Regarding heat transfer characteristics, it is clear that the nanofluids produce a significant enhancement in heat transfer when compared to conventional fluids.
- But, both the Maxwell-Garnett model [57] based on effective medium theory and Murugesan et al. [58] based on Brownian motion and interfacial layer formation, used in Cases 1 and 2, respectively, under predict the heat transfer enhancement to a large extent when compared to experimental data of effective thermal conductivity and viscosity considered in Case 3. Also, there is a considerable variation even between those two models.

Thus, we can understand that the choice of effective property models have a significant effect on the prediction of flow and heat transfer characteristics of nanofluids. A completely contradicting flow phenomenon is displayed in Cases 1 and 2 due to variations in models. The effects of uncertainties are expected to produce higher variations in flow and heat transfer characteristics of nanofluids in free and combined convection scenarios, as there will be an interaction between the flow and heat transfer characteristics. Thus, it is clear that the choice of effective property models play an important role in assessing the flow characteristics and heat transfer potential of nanofluids for real time applications.

Acknowledgment

One of the authors, S. Dhinakaran, gratefully acknowledges the financial aid received from Science and Engineering Research Board, Department of Science & Technology (DST), Government of India through a project grant (Project Reference No. SB/FTP/ETA-427/2012) for carrying out this work. The authors are highly obliged to the reviewers for their insightful comments and suggestions.

References

[1] S.U.S. Choi, Enhancing thermal conductivity of fluids with nanoparticles, ASME Publ. FED 231 (1995) 99–106.
[2] S. Lee, S.U.S. Choi, Application of metallic nanoparticle suspensions in advanced cooling systems, Tech. Rep. Argonne National Lab., IL (United States), 1996.
[3] K.V. Wong, O. De Leon, Applications of nanofluids: current and future, Adv. Mech. Eng. 2 (2010) 519659.
[4] R. Taylor, S. Coulombe, T. Otanicar, P. Phelan, A. Gunawan, W. Lv, G. Rosengarten, R. Prasher, H. Tyagi, Small particles, big impacts: a review of the diverse applications of nanofluids, J. Appl. Phys. 113 (1) (2013) 011301.
[5] O. Mahian, A. Kianifar, S.A. Kalogirou, I. Pop, S. Wongwises, A review of the applications of nanofluids in solar energy, Int. J. Heat Mass Transf. 57 (2) (2013) 582–594.
[6] O. Abouali, G. Ahmadi, Computer simulations of natural convection of single phase nanofluids in simple enclosures: a critical review, Appl. Therm. Eng. 36 (2012) 1–13.
[7] A. Kamyar, R. Saidur, M. Hasanuzzaman, Application of computational fluid dynamics (CFD) for nanofluids, Int. J. Heat Mass Transf. 55 (15) (2012) 4104–4115.
[8] S.E.B. Maiga, S.J. Palm, C.T. Nguyen, G. Roy, N. Galanis, Heat transfer enhancement by using nanofluids in forced convection flows, Int. J. Heat Fluid Flow 26 (4) (2005) 530–546.
[9] M. Sheikholeslami, K. Vajravelu, M.M. Rashidi, Forced convection heat transfer in a semi annulus under the influence of a variable magnetic field, Int. J. Heat Mass Transf. 92 (2016) 339–348.
[10] M. Sheikholeslami, M. Rashidi, D. Ganji, Effect of non-uniform magnetic field on forced convection heat transfer of water nanofluid, Comput. Methods Appl. Mech. Eng. 294 (2015) 299–312.
[11] M. Sheikholeslami, M. Rashidi, T. Hayat, D. Ganji, Free convection of magnetic nanofluid considering MFD viscosity effect, J. Mol. Liq. 218 (2016) 393–399.
[12] M. Sheikholeslami, H. Ashorynejad, P. Rana, Lattice Boltzmann simulation of nanofluid heat transfer enhancement and entropy generation, J. Mol. Liq. 214 (2016) 86–95.
[13] M. Sheikholeslami, M. Rashidi, Ferrofluid heat transfer treatment in the presence of variable magnetic field, Eur. Phy. J. Plus 130 (6) (2015) 1–12.
[14] M. Sheikholeslami, A.J. Chamkha, Flow and convective heat transfer of a ferro-nanofluid in a double-sided lid-driven cavity with a wavy wall in the presence of a variable magnetic field, Numerical Heat Transfer Part A Appl. 69 (10) (2016) 1186–1200.
[15] M.S. Kandelousi, KKL correlation for simulation of nanofluid flow and heat transfer in a permeable channel, Phys. Lett. A 378 (45) (2014) 3331–3339.
[16] M. Sheikholeslami, D.D. Ganji, Ferrohydrodynamic and magnetohydrodynamic effects on ferrofluid flow and convective heat transfer, Energy 75 (2014) 400–410.
[17] M. Sheikholeslami, D. Ganji, Heat transfer of Cu-water nanofluid flow between parallel plates, Powder Technol. 235 (2013) 873–879.
[18] M.M. Zdravkovich, Flow around Circular Cylinders: Volume 2: Applications, vol. 2, Oxford University Press, 2003.
[19] M.S. Valipour, A.Z. Ghadi, Numerical investigation of fluid flow and heat transfer around a solid circular cylinder utilizing nanofluid, Int. Commun. Heat Mass Transfer 38 (9) (2011) 1296–1304.
[20] R.L. Hamilton, O.K. Crosser, Thermal conductivity of heterogeneous two-component systems, Ind. Eng. Chem. Fundam. 1 (3) (1962) 187–191.
[21] H.C. Brinkman, The viscosity of concentrated suspensions and solutions, J. Chem. Phys. 20 (4) (1952) 571.
[22] M.S. Valipour, R. Masoodi, S. Rashidi, M. Bovand, M. Mirhosseini, A numerical study on convection around a square cylinder using Al_2O_3-H_2O nanofluid, Therm. Sci. 18 (4) (2014) 1305–1314.
[23] M. Vegad, S. Satadia, P. Pradip, P. Chirag, P. Bhargav, Heat transfer characteristics of low Reynolds number flow of nanofluid around a heated circular cylinder, Procedia Technol. 14 (2014) 348–356.
[24] J.C.M. Garnett, Colours in metal glasses, in metallic films, and in metallic solutions, II, Philosophical Transactions of the Royal Society of London. Series A, Containing Papers of a Mathematical or Physical Character 1906, pp. 237–288.
[25] E. Abu-Nada, K. Ziyad, M. Saleh, Y. Ali, Heat transfer enhancement in combined convection around a horizontal cylinder using nanofluids, J. Heat Transf. 130 (8) (2008) 084505.
[26] R.T.H. Bing, H.A. Mohammed, Upward laminar flow around a circular cylinder using nanofluids, J. Purity, Util. React. Environ. 1 (2012) 435–450.
[27] V. Etminan-Farooji, E. Ebrahimnia-Bajestan, H. Niazmand, S. Wongwises, Unconfined laminar nanofluid flow and heat transfer around a square cylinder, Int. J. Heat Mass Transf. 55 (5) (2012) 1475–1485.
[28] A.J. Chamkha, A.M. Rashad, A.M. Aly, Transient natural convection flow of a nanofluid over a vertical cylinder, Meccanica 48 (1) (2013) 71–81.
[29] S. Sarkar, A. Dalal, G. Biswas, Unsteady wake dynamics and heat transfer in forced and mixed convection past a circular cylinder in cross flow for high Prandtl numbers, Int. J. Heat Mass Transf. 54 (15) (2011) 3536–3551.
[30] S. Sarkar, S. Ganguly, G. Biswas, Mixed convective heat transfer of nanofluids past a circular cylinder in cross flow in unsteady regime, Int. J. Heat Mass Transf. 55 (17) (2012) 4783–4799.
[31] S. Sarkar, S. Ganguly, A. Dalal, Buoyancy driven flow and heat transfer of nanofluids past a square cylinder in vertically upward flow, Int. J. Heat Mass Transf. 59 (2013) 433–450.
[32] S. Sarkar, S. Ganguly, A. Dalal, P. Saha, S. Chakraborty, Mixed convective flow stability of nanofluids past a square cylinder by dynamic mode decomposition, Int. J. Heat Fluid Flow 44 (2013) 624–634.
[33] S. Sarkar, S. Ganguly, A. Dalal, Analysis of entropy generation during mixed convective heat transfer of nanofluids past a rotating circular cylinder, J. Heat Transf. 136 (6) (2014) 062501.
[34] A. Behzadmehr, M. Saffar-Avval, N. Galanis, Prediction of turbulent forced convection of a nanofluid in a tube with uniform heat flux using a two phase approach, Int. J. Heat Fluid Flow 28 (2) (2007) 211–219.
[35] A. Akbarinia, R. Laur, Investigating the diameter of solid particles effects on a laminar nanofluid flow in a curved tube using a two phase approach, Int. J. Heat Fluid Flow 30 (4) (2009) 706–714.
[36] M. Esfandiary, B. Mehmandoust, A. Karimipour, H.A. Pakravan, Natural convection of Al_2O_3-water nanofluid in an inclined enclosure with the effects of slip velocity mechanisms: Brownian motion and thermophoresis phenomenon, Int. J. Therm. Sci. 105 (2016) 137–158.
[37] O. Ghaffari, A. Behzadmehr, H. Ajam, Turbulent mixed convection of a nanofluid in a horizontal curved tube using a two-phase approach, Int. Commun. Heat Mass Transfer 37 (10) (2010) 1551–1558.
[38] M. Goodarzi, M.R. Safaei, K. Vafai, G. Ahmadi, M. Dahari, S.N. Kazi, N. Jomhari, Investigation of nanofluid mixed convection in a shallow cavity using a two-phase mixture model, Int. J. Therm. Sci. 75 (2014) 204–220.
[39] H.A. Pakravan, M. Yaghoubi, Analysis of nanoparticles migration on natural convective heat transfer of nanofluids, Int. J. Therm. Sci. 68 (2013) 79–93.
[40] M. Siavashi, M. Jamali, Heat transfer and entropy generation analysis of turbulent flow of TiO_2-water nanofluid inside annuli with different radius ratios using two-phase mixture model, Appl. Therm. Eng. 100 (2016) 1149–1160.
[41] V. Bianco, F. Chiacchio, O. Manca, S. Nardini, Numerical investigation of nanofluids forced convection in circular tubes, Appl. Therm. Eng. 29 (17) (2009) 3632–3642.
[42] S. Rashidi, M. Bovand, J.A. Esfahani, G. Ahmadi, Discrete particle model for convective Al_2O_3-water nanofluid around a triangular obstacle, Appl. Therm. Eng. 100 (2016) 39–54.
[43] M. Akbari, N. Galanis, A. Behzadmehr, Comparative assessment of single and two-phase models for numerical studies of nanofluid turbulent forced convection, Int. J. Heat Fluid Flow 37 (2012) 136–146.
[44] M. Sheikholeslami, D. Ganji, M. Rashidi, Magnetic field effect on unsteady nanofluid flow and heat transfer using Buongiorno model, J. Magn. Magn. Mater. 416 (2016) 164–173.
[45] M. Sheikholeslami, T. Hayat, A. Alsaedi, MHD free convection of *Al* 2 O 3–water nanofluid considering thermal radiation: a numerical study, Int. J. Heat Mass Transf. 96 (2016) 513–524.
[46] M. Sheikholeslami, M. Rashidi, Non-uniform magnetic field effect on nanofluid hydrothermal treatment considering Brownian motion and thermophoresis effects, J. Braz. Soc. Mech. Sci. Eng. 38 (4) (2016) 1171–1184.
[47] M. Sheikholeslami, M. Rashidi, D. Ganji, Numerical investigation of magnetic nanofluid forced convective heat transfer in existence of variable magnetic field using two phase model, J. Mol. Liq. 212 (2015) 117–126.
[48] M. Sheikholeslami, D.D. Ganji, Nanofluid flow and heat transfer between parallel plates considering Brownian motion using DTM, Comput. Methods Appl. Mech. Eng. 283 (2015) 651–663.
[49] M. Sheikholeslami, M. Gorji-Bandpy, D. Ganji, S. Soleimani, Thermal management for free convection of nanofluid using two phase model, J. Mol. Liq. 194 (2014) 179–187.
[50] W. Daungthongsuk, S. Wongwises, A critical review of convective heat transfer of nanofluids, Renew. Sust. Energ. Rev. 11 (5) (2007) 797–817.
[51] S. Kakaç, A. Pramuanjaroenkij, Single-phase and two-phase treatments of convective heat transfer enhancement with nanofluids–a state-of-the-art review, Int. J. Therm. Sci. 100 (2016) 75–97.
[52] S. Kakac, A. Pramuanjaroenkij, Review of convective heat transfer enhancement with nanofluids, Int. J. Heat Mass Transf. 52 (13) (2009) 3187–3196.
[53] S. Özerinç, S. Kakaç, A.G. Yazcoğlu, Enhanced thermal conductivity of nanofluids: a state-of-the-art review, Microfluid. Nanofluid. 8 (2) (2010) 145–170.
[54] E. Abu-Nada, Effects of variable viscosity and thermal conductivity of CuO-water nanofluid on heat transfer enhancement in natural convection: mathematical model and simulation, J. Heat Transf. 132 (5) (2010) 052401.

[55] I.M. Mahbubul, R. Saidur, M.A. Amalina, Latest developments on the viscosity of nanofluids, Int. J. Heat Mass Transf. 55 (4) (2012) 874–885.
[56] Y. Xuan, Q. Li, Investigation on convective heat transfer and flow features of nanofluids, J. Heat Transf. 125 (1) (2003) 151–155.
[57] J. C. Maxwell, Clarendon Press, Oxford, 1873.
[58] C. Murugesan, S. Sivan, Limits for thermal conductivity of nanofluids, Therm. Sci. 14 (1) (2010) 65–71.
[59] H. Chen, Y. Ding, Y. He, C. Tan, Rheological behaviour of ethylene glycol based titania nanofluids, Chem. Phys. Lett. 444 (4) (2007) 333–337.
[60] W. Duangthongsuk, S. Wongwises, Measurement of temperature-dependent thermal conductivity and viscosity of TiO 2-water nanofluids, Exp. Thermal Fluid Sci. 33 (4) (2009) 706–714.
[61] Y. Xuan, W. Roetzel, Conceptions for heat transfer correlation of nanofluids, Int. J. Heat Mass Transf. 43 (19) (2000) 3701–3707.
[62] A. Sohankar, C. Norberg, L. Davidson, Int. J. Numer. Methods Fluids 26 (1) (1998) 39–56.
[63] S. Dhinakaran, Heat transport from a bluff body near a moving wall at $Re = 0$, Int. J. Heat Mass Transf. 54 (2526) (2011) 5444–5458.
[64] J. Eapen, R. Rusconi, R. Piazza, S. Yip, The classical nature of thermal conduction in nanofluids, J. Heat Transf. 132 (10) (2010) 102402.
[65] J. Buongiorno, D.C. Venerus, N. Prabhat, T. McKrell, J. Townsend, R. Christianson, Y.V. Tolmachev, P. Keblinski, L.-w. Hu, J.L. Alvarado, et al., A benchmark study on the thermal conductivity of nanofluids, J. Appl. Phys. 106 (9) (2009) 094312.
[66] P. Keblinski, S.R. Phillpot, S.U.S. Choi, J.A. Eastman, Mechanisms of heat flow in suspensions of nano-sized particles (nanofluids), Int. J. Heat Mass Transf. 45 (4) (2002) 855–863.
[67] S. Patankar, Numerical Heat Transfer and Fluid Flow, CRC Press, 1980.
[68] B.P. Leonard, A stable and accurate convective modelling procedure based on quadratic upstream interpolation, Comput. Methods Appl. Mech. Eng. 19 (1) (1979) 59–98.
[69] R.P. Bharti, R.P. Chhabra, V. Eswaran, A numerical study of the steady forced convection heat transfer from an unconfined circular cylinder, Heat Mass Transf. 43 (7) (2007) 639–648.
[70] R.P. Bharti, R.P. Chhabra, V. Eswaran, Steady forced convection heat transfer from a heated circular cylinder to power-law fluids, Int. J. Heat Mass Transf. 50 (5) (2007) 977–990.
[71] M. Braza, P.H.H.M. Chassaing, H.H. Minh, Numerical study and physical analysis of the pressure and velocity fields in the near wake of a circular cylinder, J. Fluid Mech. 165 (1986) 79–130.
[72] S.C.R. Dennis, G.-Z. Chang, Numerical solutions for steady flow past a circular cylinder at Reynolds numbers up to 100, J. Fluid Mech. 42 (03) (1970) 471–489.
[73] S. Bhattacharyya, S. Dhinakaran, A. Khalili, Fluid motion around and through a porous cylinder, Chem. Eng. Sci. 61 (13) (2006) 4451–4461.
[74] B. Fornberg, A numerical study of steady viscous flow past a circular cylinder, J. Fluid Mech. 98 (04) (1980) 819–855.
[75] C.F. Lange, F. Durst, M. Breuer, Momentum and heat transfer from cylinders in laminar crossflow at $10^{-14} \le Re \le 200$, Int. J. Heat Mass Transf. 41 (22) (1998) 3409–3430.
[76] A.A. Soares, J.M. Ferreira, R.P. Chhabra, Flow and forced convection heat transfer in crossflow of non-Newtonian fluids over a circular cylinder, Ind. Eng. Chem. Res. 44 (15) (2005) 5815–5827.
[77] R.A. Ahmad, Z.H. Qureshi, Laminar mixed convection from a uniform heat flux horizontal cylinder in a crossflow, J. Thermophys. Heat Transf. 6 (2) (1992) 277–287.
[78] A.K. Dhiman, R.P. Chhabra, A. Sharma, V. Eswaran, Effects of Reynolds and Prandtl numbers on heat transfer across a square cylinder in the steady flow regime, Numer. Heat Transfer, Part A: Appl. 49 (7) (2006) 717–731.